2022-05-18

Human APOER2 isoforms have differential cleavage events and synaptic properties

Cellular/Molecular

Human APOER2 Isoforms Have Differential Cleavage Events and Synaptic Properties

Kerilyn Casey Omuro, Christina M. Gallo, Lauren Scrandis, Angela Ho, and Uwe Beffert
Department of Biology, Boston University, Boston, Massachusetts 02215

Human apolipoprotein E receptor 2 (APOER2) is a type I transmembrane protein with a large extracellular domain (ECD) and a short cytoplasmic tail. APOER2-ECD contains several ligand-binding domains (LBDs) that are organized into exons with aligning phase junctions, which allows for in-frame exon cassette splicing events. We have identified 25 human APOER2 isoforms from cerebral cortex using gene-specific APOER2 primers, where the majority are exon-skipping events within the N-terminal LBD regions compared with six identified in the heart. APOER2 undergoes proteolytic cleavage in response to ligand binding that releases a C-terminal fragment (CTF) and transcriptionally active intracellular domain (ICD). We tested whether the diversity of human brain-specific APOER2 variants affects APOER2 cleavage. We found isoforms with differing numbers of ligand-binding repeats generated different amounts of CTFs compared with full-length APOER2 (APOER2-FL). Specifically, APOER2 isoforms lacking exons 5–8 (Δex5–8) and lacking exons 4–6 (Δex4–6) generated the highest and lowest amounts of CTF generation, respectively, in response to APOE peptide compared with APOER2-FL. The differential CTF generation of Δex5–8 and Δex4–6 coincides with the proteolytic release of the ICD, which mediates transcriptional activation facilitated by the Mint1 adaptor protein. Functionally, we demonstrated loss of mouse *Apoer2* decreased miniature event frequency in excitatory synapses, which may be because of a decrease in the total number of synapses and/or VAMP2 positive neurons. Lentiviral infection with human APOER2-FL or Δex4–6 isoform in *Apoer2* knockout neurons restored the miniature event frequency but not Δex5–8 isoform. These results suggest that human APOER2 isoforms have differential cleavage events and synaptic properties.

Key words: APOE; APOER2; cleavage; splicing; synaptic

Significance Statement

Humans and mice share virtually the same number of protein-coding genes. However, humans have greater complexity of any higher eukaryotic organisms by encoding multiple protein forms through alternative splicing modifications. Alternative splicing allows pre-mRNAs transcribed from genes to be spliced in different arrangements, producing structurally and functionally distinct protein variants that increase proteomic diversity and are particularly prevalent in the human brain. Here, we identified 25 distinct human APOER2 splice variants from the cerebral cortex using gene-specific APOER2 primers, where the majority are exon-skipping events that exclude N-terminal ligand-binding regions of APOER2. We show that some of the APOER2 variants have differential proteolytic properties in response to APOE ligand and exhibit distinct synaptic properties.

Introduction

Human apolipoprotein E receptor 2 (APOER2, official gene name *LRP8*) is enriched in the brain and displays a high degree of cassette exon splicing events where inclusion or skipping of an exon will insert or delete a sequence from the final mRNA (Kim et al., 1996; Clatworthy et al., 1999; Gallo et al., 2020, 2022). Similarly, mouse *Apoer2* is one of the top neuronal genes related to cell-type exon skipping events (Zhang et al., 2014). Human APOER2 is composed of five functionally distinct domains including the ligand-binding domain (LBD), which consists of two types of repeats, LDL receptor type A (LDLa, exons 2–6) and epidermal growth factor (EGF) precursor-like repeats (exons 7–8 and 14) that bind extracellular ligands such as Reelin and APOE (Brandes et al., 1997; reviewed in Dlugosz and Nimpf, 2018; Fig.

Received Sep. 3, 2021; revised Mar. 24, 2022; accepted Apr. 6, 2022.

Author contributions: K.C.O., C.M.G., A.H., and U.B. designed research; K.C.O., C.M.G., and L.S. performed research; K.C.O., L.S., A.H., and U.B. analyzed data; K.C.O., A.H., and U.B. wrote the paper.

This work was supported by the National Institute of Aging Grants AG059762 to U.B. and AG069498 to C.M.G., the Harold and Margaret Southerland Alzheimer's Research Fund, National Institute of General Medical Sciences T32 Training Grant in Biomolecular Pharmacology GM008541 to K.C.O. and C.M.G., and the National Science Foundation Grant DGE-1247312 to K.C.O. The Genotype-Tissue Expression (GTEx) Project was supported by the Common Fund of the Office of the Director of the National Institutes of Health, and by NCI, NHGRI, NHLBI, NIDA, NIMH, and NINDS. We thank Dr. Joachim Herz and Dr. Thomas C. Südhof for antibodies and members of the lab for comments and advice.

The authors declare no competing financial interests.

Correspondence should be addressed to Angela Ho at aho1@bu.edu or Uwe Beffert at ub1@bu.edu.

https://doi.org/10.1523/JNEUROSCI.1800-21.2022

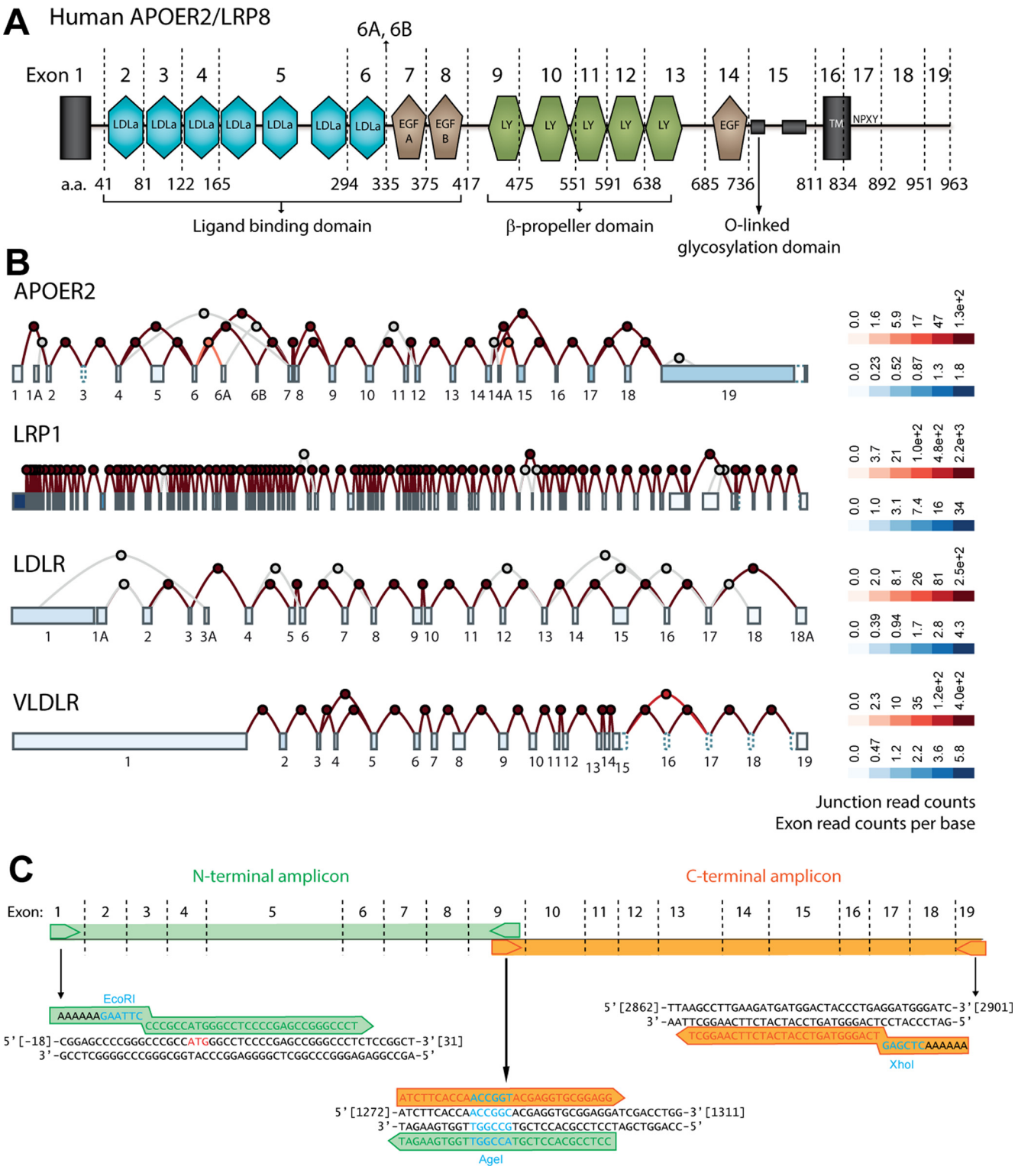

Figure 1. Structure of human APOER2. ***A***, APOER2 is a type I transmembrane (TM) protein with a large extracellular domain and a short cytoplasmic tail. Functional domains are indicated by color, including the extracellular LDLa (blue) and EGF repeats (brown) that make up the ligand-binding domain. The LY repeats (green) form the beta-propeller domain. Exon 1 encodes the signal peptide. Exon 15 contains the O-linked glycosylation domain. Exons 16 and 17 include the hydrophobic residues that encompassed the TM domain and conserved endocytic NPxY motif. The dotted lines indicate exon boundaries. Bottom, The amino acid positions. ***B***, Schematic diagram from https://GTExportal.org representing human exon-level RNAseq data for LDLR family from frontal cortex. Boxes represent specific exons and are color coded based on relative expression, with higher expressed exons in dark blue and low expressed exons in white. Exon junctions are indicated by colored circles above the exons; dark red indicates high usage, whereas white indicates low usage. (GTEx Analysis Release V8 dbGaP Accession phs000424.v8.p2; Brain - Cortex the GTEx Portal on 03/24/2021). ***C***, Schematic diagram illustrating the APOER2 PCR amplification scheme. The N-terminal (~1307 bp) and C-terminal (~1614 bp) ORFs of APOER2 were amplified independently from mRNA isolated from human cerebral cortex and heart using gene-specific primers by RT-PCR. N-terminal primers (green) encompassed exons 1–9, and C-terminal primers (orange) encompassed exons 9–19 with internal AgeI site within exon 9. Both external EcoRI and XhoI restriction sites were designed for cloning.

1*A*). Adjacent to the ligand-binding domain are five LDL receptor class B (LY) repeats (exons 9–13) that form the β-propeller domain, which is critical for ligand release and receptor recycling (Rudenko et al., 2002). The third domain (exon 15) contains clustered O-linked carbohydrate chains critical for receptor sorting to the cell surface and stabilization (Kim et al., 1996; Wasser et al., 2014). The fourth domain is the hydrophobic transmembrane region (exons 16–17) and the fifth domain is the cytoplasmic tail (exon 18–19) that directs the receptor to clathrin-coated pits necessary for endocytosis and binds cytosolic adaptor proteins (Kim et al., 1996; Novak et al., 1996; Brandes et al., 1997; Gotthardt et al., 2000; Stockinger et al., 2000; Hoe et al., 2006; He et al., 2007; Myant, 2010).

Most of the splicing events in mouse *Apoer2* occur in functionally important domains such as the LBD (Brandes et al., 2001; Hibi et al., 2009), the O-linked sugar domain (May et al., 2003; Wasser et al., 2014), or the cytoplasmic signaling tail (Beffert et al., 2005, 2006). For example, Reelin-mediated enhancement of long-term potentiation depends on the presence of the alternative spliced exon 19 of mouse *Apoer2*, which encodes the cytoplasmic insert (Beffert et al., 2005). Mice lacking *Apoer2* exon 19 perform poorly in learning and memory tasks, demonstrating the importance of Reelin in conjunction with regulated alternative splicing of *Apoer2* associated with synaptic function (Beffert et al., 2005). Supporting studies showed Reelin binding to Apoer2 triggers epigenetic changes of neuronal enhancers required for transcriptional regulation of synaptic plasticity genes during memory formation (Telese et al., 2015). This epigenetic signature requires γ-secretase cleavage of Apoer2, revealing a critical role for the Apoer2 intracellular domain in regulating synaptic-generated signals (Telese et al., 2015). However, the role of APOE-APOER2 signaling in receptor proteolysis and synaptic function in naturally occurring human APOER2 splice variants remains largely unexplored.

Here, we amplified the N-terminal and C-terminal open-reading frame (ORF) of *APOER2* using gene-specific APOER2 primers from normal adult human cerebral cortex or heart mRNA. We identified a large number of in-frame APOER2 products from brain compared with the heart. The majority of human APOER2 from heart was represented by the full-length APOER2 (APOER2-FL) isoform. Meanwhile, APOER2 lacking exon 5 (Δex5), which contains three ligand-binding repeats, APOER2 lacking exons 5 and 8 (Δex5, Δex8), and APOER2-FL were predominantly expressed in the brain. In fact, most of the other APOER2 clones lacked exon 5 in combination with other skipped exons, suggesting an important role for exon 5 in the brain. For the C-terminal APOER2 clones, we confirmed common splice variants skipping exons 15 and 18. We systematically tested a number of APOER2 splice variants lacking various LBDs and found APOER2 splice variants influence APOER2 receptor processing, transcriptional activation, and basal synaptic transmission.

Materials and Methods

Human APOER2 splice variant screen. The APOER2 splice variant constructs were derived from a PCR-based screen of cDNA isolated from adult human normal cerebral cortex and heart (Invitrogen). Because of the large size of the *APOER2* coding sequence (2892 bp), we amplified the N-terminal open reading frame (~1307 bp) using a 5′ primer (AAAAAA*GAATTC*CCCCGCCATGGGCCTCCCCGAGCCGGGCCCT) with EcoRI before the Kozak and ATG start site at 6 bp and a 3′ primer (CCTCCGCACCTCGT*ACCGGT*TGGTGAAGAT) with AgeI in the middle of *APOER2* at 1272 bp. We then amplified the C-terminal ORF (~1614 bp) using a 5′ primer (ATCTTCACCA*ACCGGT*ACGAGGT GCGGAGG) with AgeI, which overlapped with the above sequence, and a 3′ primer (AAAAAA*CTCGAG*TCAGGGTAGTCCATCATCTTCAAGG CT) with XhoI after the *APOER2* termination signal at 2892 bp. The PCR fragments were TOPO-TA cloned (Thermo Fisher Scientific) and subcloned together using the EcoRI-AgeI-XhoI restriction sites to form full-length APOER2 constructs and subsequently subcloned into the pcDNA3 vector (Invitrogen).

Plasmids. To generate the GFP-tagged APOER2 splice variants, we PCR amplified APOER2 from the full-length pcDNA3 constructs as described above using a 5′ primer (AAAAGTCGACATGGGCCTCC CCGAGCCGGGCCCTCTCCGG) with SalI before the ATG start site and 3′ primer (CCCCGGATCCGGGTAGTCCATCATCTTCAAGGC TTAATGC) with BamHI site and subcloned into pEGFP-N3 vector (Clontech Laboratories) using the SalI and BamHI sites. The lentiviral APOER2 constructs were subcloned into the untagged pFUW vector using the XbaI and EcoRI sites and generating pFUW-APOER2-FL, pFUW–APOER2–Δex5–8, and pFUW–APOER2–Δex4–6 for lentiviral production. For the transactivation plasmids, the luciferase and β-galactosidase plasmids were previously described (Cao and Südhof, 2001), and eukaryotic expression vectors containing Gal4 or Gal4/VP16 were based on pMst (Gal4) or pMst-GV (Gal4/VP16), which is derived from the mammalian expression pM vector (Clontech Laboratories). We first generated pMst-APOER2-ICD, pMst-GV-APOER2-ICD by cloning the intracellular domain of APOER2-FL (APOER2-ICD, residues 849–964) into the BamHI and SalI sites of pMst or pMst-GV. The APOER2-ICD was amplified using the following 5′ primer (AAAA*GGATCC*AAAGA AACTGGAAGCGGAAGAACA) with BamHI site and 3′ primer (CCCC*GTCGAC*GTCAGGGTAGTCCATCATCTTCAAGGCTTAAT-GC) with SalI site. Next, we amplified the appropriate APOER2-ECD using the following 5′ primer (AAAA*CCATGG*ATGGGCCTCCCCGA GCCGGGCCCTCTCCGG) with NcoI site and 3′ primer (CCCC*GCT AGC*AACCAGATCAGGTATCCACTCATG) with NheI site for APOER2-FL, Δex5–8 or Δex4–6. The APOER2-ECD PCR fragments were subcloned into the NcoI and NheI sites of the pMst-APOER2-ICD, pMst-GV-APOER2-ICD to obtain the final pMst-APOER2-FL, pMst–APOER2–Δex5–8, pMst–APOER2–Δex4–6, pMst-GV-APOER2-FL, pMst–GV–APOER2–Δex5–8, and pMst–GV–APOER2–Δex4–6 used for the transactivation assay.

Primary murine neuronal cultures. Primary hippocampal and cortical neuronal cultures were prepared from individual newborn *Apoer2* mice of either sex that were from a cross of a heterozygous *Apoer2* male with a homozygous *Apoer2* female (B6;129S6-*Lrp8*^{tm1Her}/J, stock #003524, The Jackson Laboratory) as previously described (Kavalali et al., 1999). All animal experiments were approved by the Boston University Institutional Animal Care and Use Committee, and methods were performed in accordance with relevant guidelines and regulations. Briefly, the cortex and the hippocampi were independently dissected out from each individual mouse and dissociated with trypsin for 10 min at 37° C, triturated and plated with plating medium onto precoated Matrigel (Corning) coverslips (BD Biosciences) and placed in 24-well plates. Neurons were maintained in humidified incubator with 5% CO_2 at 37°C.

Lentivirus preparation and infection of neuronal cultures. Recombinant lentivirus was produced by transfecting HEK293T cells as described previously (Chaufty et al., 2012). Briefly, HEK293T cells were cotransfected with lentiviral pFUW plasmids for APOER2-FL and APOER2 Δex5–8 or Δex4–6 with viral enzymes and envelope proteins (pRSV/REV, pMDLg/RRE, and pVSV-G) using FuGENE6 reagent (Roche). The initial media was changed into neuronal growth media after 6 h of transfection. Lentivirus-containing conditioned media were harvested 48 h after transfection, filtered to remove debris, aliquoted, and stored at −80°C. Primary murine neurons were infected at 2 d *in vitro* (DIV) and maintained throughout until experiment.

Luciferase transactivation assay. The luciferase transactivation assay was conducted using the constructs previously described (Biederer et al., 2002). Briefly, a 24-well plate of COS7 cells at 50–80% confluency was cotransfected using FuGENE6 (Roche) with the following plasmids: pG5E1B-luc, pCMV-LacZ, pMst (Gal4), or pMst-GV (Gal4/VP16) construct for the receptor of interest (pMst-APOER2-FL, pMst–

APOER2–Δex5–8, pMst–APOER2–Δex4–6, pMst–GV–APOER2–FL, pMst-GV-APOER2 Δex5–8, pMst-GV-APOER2 Δex4–6, or pMs-APP). For the adaptor screen, COS7 cells were transfected with pCMV, pCMV-Dab1, pCMV-Dab2, pCMV-JIP1, pCMV-JIP2, pCMV-Mint1, pCMV-Mint2, pCMV-Tip60, pCMV-Fe65, or pCMV-PSD95 (gifts from Thomas Südhof and Joachim Herz's laboratory). In experiments with DAPT, cells were treated with 1 μM of DAPT for 24 h before collection. Cells were harvested 48–72 h after transfection in 100 µl reporter lysis buffer (Promega) and freeze thawed to achieve cell lysis. The resulting lysates were spun down at 15,000 × *g* for 1 min, then split into 20 µl for the luciferase assay and 30 µl for the β-galactosidase assay, and the remainder reserved for validation. Luciferase activity was measured on the Victor3 luminescence plate reader (PerkinElmer) directly following application of the luciferase reagent (Promega), and β-galactosidase was measured in a colorimetric plate reader (Bio-Rad) following the mammalian β-galactosidase assay kit (Thermo Fisher Scientific). For quantifications, the luciferase activity was standardized by the β-galactosidase activity to control for transfection efficiency, and the resulting data were normalized by using the transactivation activity from Gal4 alone (pMst) as the baseline. Transactivation assays were performed in duplicates and replicated at least two times.

Biochemical analysis and quantitative immunoblotting. HEK293T or COS7 cells were transfected with various APOER2 splice variants individually using FuGENE6 reagent (Roche). For DAPT treatment, 25 mM stock solution of DAPT (Calbiochem) in DMSO was added to the final concentration as specified in the figure legends. DMSO served as the vehicle control. For APOE mimetic peptide treatment, the lyophilized peptide (LRVRLASHLRKLRKRLL, Peptide 2.0) was reconstituted in PBS (20 mM stock) and stored in −20°C in single-use aliquots, and PBS was used as vehicle control. After 48 h, cell lysates were collected in sample buffer containing 200 mM Tris-Cl, pH 6.8, 8% SDS, 0.4% bromophenol blue, and 40% glycerol, and boiled in the presence of 1% β-mercaptoethanol for 10 min. Proteins were analyzed by SDS-PAGE and transferred onto nitrocellulose membranes using the Trans-Blot tank transfer system (Bio-Rad) at 400 mA for 2 h at 4°C. Membranes were blocked in LI-COR blocking buffer for 1 h and incubated overnight at 4°C with the following primary antibodies diluted in LI-COR blocking buffer: 2561, rabbit anti-APOER2 C-terminal (gift from Joachim Herz's laboratory, 1:1000), rabbit anti-APOER2 (1:1000; Abcam), mouse anti-GAPDH (1:2000; EMD Millipore), rabbit anti-GFP (1:500; Synaptic Systems). Membranes were subsequently washed with PBS and incubated for 1 h at room temperature with the compatible immunoreactive (IR) dye secondary antibodies diluted in LI-COR blocking buffer IRDye 680RD goat anti-rabbit, IRDye 800CW goat anti-mouse (1:10,000; LI-COR). Quantitative analysis was performed using the Odyssey Infrared Imager CLx scanner and Image Studio 5.2.5 software (LI-COR). Signals were quantified in the Image Studio software (LI-COR).

Immunoprecipitation. COS7 cells were cotransfected with GFP-Mint1 and individual APOER2 constructs for 48 h. Cells were collected in cold immunoprecipitation (IP) buffer containing the following: 20 mM Tris HCl, pH 8.0, 100 mM NaCl, 1 mM EDTA, pH 8.0, and 1% NP-40) with fresh additions of protease and phosphatase inhibitors (Biotool). The cell suspension was passed through a 28-gauge syringe, and the lysate was centrifuged in a microcentrifuge at 21,000 × *g* for 20 min and subjected to 2 h of immunoprecipitation using rabbit anti-GFP (1:500; Synaptic Systems) followed by an overnight incubation with protein A Ultralink resin (Thermo Fisher Scientific). The resin was washed 3–5 times with IP buffer and boiled for 10 min in reducing SDS sample buffer to collect precipitated proteins.

Surface biotinylation. COS7 cells were transfected with APOER2-FL, Δex5-8, or Δex4-6 plasmids using FuGENE6 transfection reagent. After 48 h, cells were incubated with 1 mg/ml sulfo-NHS-LC-Biotin (Thermo Fisher Scientific) in PBS for 20 min on ice, quenched with Tris-buffered saline (150 mM NaCl and 50 mM Tris, pH 7.5), and lysed with RIPA buffer containing the following: 65 mM Tris, pH 7.4, 150 mM NaCl, 1% Triton, 0.1% SDS, 0.5% Na-deoxycholate, 1 mM EDTA, pH 8.0, 50 mM NaH_2PO_4, 50 mM NaF, 10 mM Na_4P2O_7, 1 mM Na_3VO_4, and Protease Inhibitor Cocktail (Biotool). Biotinylated surface proteins were precipitated with RIPA-equilibrated NeutrAvidin beads (50:50 slurry; Thermo Fisher Scientific) overnight at 4°C with gentle rocking to precipitate the biotinylated proteins. Beads were washed with RIPA buffer and spun at 800 × *g* for 1 min. Proteins were eluted from the NeutrAvidin beads by boiling for 10 min in reducing sample buffer and resolved by SDS-PAGE and immunoblotted for rabbit anti-APOER2 (1:1000; Abcam). Surface expression was determined by comparing surface APOER2 to total APOER2 protein expression levels.

Electrophysiology. Miniature excitatory postsynaptic recordings from DIV14 hippocampal neurons were placed in the recording chamber containing the recording solution containing the following (in mM): 140 NaCl, 3 KCl, 1.5 $MgCl_2$, 2.5 $CaCl_2$, 11 glucose, and 10 HEPES (305 mOsm, pH 7.4), which was supplemented with tetrodotoxin (TTX; 1 μM) to block action potentials, APV (50 μM) to block NMDARs, and bicuculline (20 μM) to block $GABA_A$ receptor-mediated currents. Whole-cell voltage-clamp recordings were taken with the membrane potential clamped at −70 mV using patch pipettes filled with intracellular solution containing the following (in mM): 110 Cs-methanesulfonate, 10 CsCl, 10 HEPES, 0.2 EGTA, 4 Mg-ATP, 0.3 Na_2-GTP, and 10 sodium phosphocreatine (295 mOsm, pH 7.4). The miniature EPSC (mEPSC) was recorded with an Axopatch 200B amplifier and a Digidata 1440A digitizer acquisition system (Molecular Devices). Subsequent analysis was conducted using Clampfit 10.7 software (Molecular Devices).

Immunocytochemistry. Primary murine hippocampal neurons cultured in a 24-well plate on 12 mm glass coverslips (Carolina Biological Supply) were briefly rinsed with PBS and fixed in 4% paraformaldehyde (Thermo Fisher Scientific) for 8 min and washed with PBS. Cells were blocked in 10% goat serum and permeabilized with 0.01% saponin in PBS for 30 min and incubated with primary antibodies in blocking buffer (10% goat serum in PBS) at 4°C overnight. Primary antibodies used included mouse anti-PSD-95 (1:250; Novus Biologicals), rabbit anti-synapsin P610 (1:250; gift from Thomas Südhof's laboratory), and mouse anti-VAMP2 (1:250; Synaptic Systems). Following PBS washes, neurons were incubated with the following fluorophore-conjugated secondary antibodies: goat anti-rabbit IgG Alexa Fluor-488 (1:500; Invitrogen) and goat anti-mouse IgG Alexa Fluor-546 (1:500; Invitrogen) for 1 h at room temperature. Coverslips were mounted on Superfrost microscope slides (Fisher Scientific) in ProLong-Gold Antifade mount with DAPI (Invitrogen) and stored at 4°C until image acquisition.

Image acquisition and analysis. Images were captured using a Carl Zeiss LSM700 scanning confocal microscope with image acquisition settings kept constant between coverslips in independent experiments, including settings for the laser gain and offset, scanning speed, and pinhole size. These settings yielded images in which the brightest pixels were not oversaturated. To assess synapse number, a single slice image was acquired of the neurons using a 63× oil objective. The region of interest was selected manually on each image using well-isolated neuronal processes. Individual puncta were quantified with the cell counter plug-in and normalized by the length of each process using National Institutes of Health ImageJ (http://imagej.nih.gov/ij) software. Colocalization between synapsin and PSD95 was determined visually and used to indicate a synapse.

Statistical analyses. All statistical analyses were performed using Prism 6 software (GraphPad) and presented as means ± SEM. Significance was set as $p < 0.05$. Experiments were repeated at least two times, and statistical information is reported in the corresponding figure legends. For *p* values for all statistical tests, see Table 6 and Extended Data Figures 2-1, 3-1, 4-1, 5-1, 6-1, 7-1.

Results

Prevalence of APOER2 splicing in human brain compared with the heart

We examined genome-wide RNAseq data from thousands of human samples through the online Genotype-Tissue Expression (GTEx) database, which provides gene expression at the exon level. Human *APOER2* had a high degree of alternative splicing events in frontal cortex, far greater than other receptors of the low-density lipoprotein receptor (LDLR) family including *LRP1*,

Table 1. Prevalence of N-terminal APOER2 clones amplified from human cerebral cortex mRNA

APOER2 splice variant	Count	Percentage
Full length	35	12.5
Δex5, Δex8	42	14.9
Δex5	38	13.5
Δex5 +ex6B	27	9.6
Δex4–6	19	6.8
Δex5–6	18	6.4
Full length +ex6B	18	6.4
Δex5–8	16	5.7
Δex4–6, Δex8	13	4.6
Δex4–5	11	3.9
Δex5, Δex7, Δex8	8	2.8
Δex8	5	1.8
Δex5–6, Δex8	5	1.8
Δex4–5, Δex8	4	1.4
Δex4, Δex5, +ex6B	3	1.1
Δex5, +ex6B, Δex7, Δex8	3	1.1
Δex5, Δex7	2	0.7
Δex5, Δex6, +ex6B	2	0.7
Δex5, +ex6B, Δex8	2	0.7
Δex3-5, +ex6B	2	0.7
Δex4, Δex5, +ex6B, Δex7	2	0.7
Δex4, Δex5, +ex6B, Δex8	2	0.7
Δex4, Δex5, +ex6B, Δex7, Δ8	2	0.7
Δex4–8	1	0.4
Δex5, +ex6B, Δex7	1	0.4
Total	281	100

Δ represents the deletion of exon, for example Δex5 is deletion of exon 5. Also, +ex6B represents inclusion of exon 6B.

LDLR, and *VLDLR* (Fig. 1*B*). Most of the splicing events were cassette exon splicing events, where inclusion or exclusion of an exon will insert or delete a sequence from the final mRNA. Also, the majority of the splicing events occur in functionally important domains such as the ligand-binding domains (exons 2–8), the O-linked glycosylation domain (exon 15), or the cytoplasmic insert (exon 18). The high level of APOER2 splicing is further supported by a study that identified genes with the most splicing events enriched in a number of mouse brain cell types, where *Apoer2* was found to be in the top neuronal genes that display cell-type splicing events (Zhang et al., 2014). However, the full extent of human APOER2 alternative splicing in brain remains unclear.

To determine the diversity of APOER2 splice variants in the adult human brain compared with other tissues, we amplified the N-terminal (~1307 bp) and C-terminal (~1614 bp) ORF of *APOER2* by RT-PCR using gene-specific primers from human cerebral cortex or heart mRNA (Fig. 1*C*). The resulting PCR products were TOPO cloned, and individual ORFs were sequenced in their entirety using vector and gene-specific primers. For N-terminal clones, we noted 281 in-frame products and a total of 25 different splice variant combinations in the human cerebral cortex. The three most common human APOER2 isoforms in the cerebral cortex were deletion of exons 5 and 8 (Δex5, Δex8, 14.9% prevalence), deletion of exon 5 (Δex 5, 13.5% prevalence) followed by the full-length isoform of APOER2 (12.5% prevalence; Table 1). Interestingly, most other N-terminal APOER2 clones lacked exon 5 in combination with other skipped exons, suggesting an important functional role for exon 5, which contains three ligand-binding LDLa repeats. In comparison, we only found 69 in-frame products and a total of six different splice variant combinations in the human heart with APOER2-FL as the most prevalent variant (68.1%; Table 2).

Table 2. Prevalence of N-terminal APOER2 clones amplified from human heart mRNA

Splice variant	Count	Percentage
Full length	47	68.1
Δex5	13	18.8
Δex5, Δex8	5	7.2
Δex5, Δex7	2	2.9
Δex8	1	1.4
Δex5, +ex6B, Δex7, Δex8	1	1.4
Total	69	100

Δ represents the deletion of exon, for example Δex5 is deletion of exon 5. Also, +ex6B represents inclusion of exon 6B.

Table 3. Prevalence of C-terminal APOER2 clones amplified from human cerebral cortex mRNA

Splice variant	Count	Percentage
Full length	6	14.3
Δex15, Δex18	16	38.1
Δex18	12	28.6
Δex15	7	16.7
Δex14, Δex15, Δex18	1	2.4
Total	42	100

Table 4. Prevalence of C-terminal APOER2 clones amplified from human heart mRNA

Splice variant	Count	Percentage
Full length	9	32.1
Δex15, Δex18	13	46.4
Δex18	4	14.3
Δex14, Δex15	2	7.1
Total	28	100

For C-terminal clones of human APOER2 found in the brain, we confirmed the existence of common splice variants lacking exon 15 (Δex15, 16.7% prevalence) and lacking exon 18 (Δex18, 28.6% prevalence), and splice variants lacking both exons 15 and 18 (Δex15, Δex18, 38.1% prevalence), as well as splice variants lacking exon 14, 15, and 18 (Δex14, Δex15, Δex18, 2.4% prevalence; Table 3). The prevalence of skipping exons 15 and 18 is of note, as both these exons play important roles in regulating synaptic plasticity as well as learning and memory (Beffert et al., 2005; Wasser et al., 2014). In total, only four and five different C-terminal variant combinations were identified from human heart and brain, respectively (Tables 3, 4). In addition, the most prevalent C-terminal APOER2 splice variant in the heart lacked both exons 15 and 18 (Δex15, Δex18, 46.4% prevalence).

In the cerebral cortex, exon 5 was the most commonly spliced out exon. Seventy-nine percent of the APOER2 isoforms either lacked exon 5 alone or in combination with other skipped exons (Table 5). Exon 5 encodes three ligand-binding LDL receptor type A repeats within the LBD, unlike the other exons (2, 3, 4 and 6) that encode a singular LDL receptor type A repeat. In addition, exon 5 contains the predicted APOE binding site based on sequence homology to the LDLR, suggesting a functional role for exon 5 (Martínez-Oliván et al., 2014). Exon 6B was also commonly excluded in 77.2% of APOER2 variants in the cerebral cortex, and nearly all APOER2 variants lacked exon 6B in the heart (98.6% excluded; Table 5). Exon 6B encodes a furin cleavage site in APOER2, and the proteolytic cleavage of APOER2

Table 5. Individual APOER2 exon splice frequency from human brain and heart tissue

Exon exclusion	Brain	Heart
ex3	0.7%	0.0%
ex4	21.4%	0.0%
ex5	79.0%	30.4%
ex6	26.3%	0.0%
ex6B	77.2%	98.6%
ex7	12.5%	4.3%
ex8	36.7%	10.1%
ex14	2.4%	7.1%
ex15	57.1%	53.6%
ex18	69.0%	60.7%

Percentages represent total N-terminal or C-terminal clones that exclude specified exon. Note exons 1, 9, and 19 are where primer sites were located, and their splicing cannot be detected using RT-PCR. Exons not listed were not detected and were excluded.

Table 6. Summary of statistical analyses, degrees of freedom, and significance for each figure

Figure	Test used	Minimum sample size	Degrees of freedom, p
2D	One-way ANOVA[a]	5	$F_{(13,125)} = 12.24$, $p < 0.0001$
3B	Two-way ANOVA[a]	3	$F_{(6,59)} = 8.773$. $p < 0.0001$ DAPT effect, $F_{(3,59)} = 79.68$, $p < 0.0001$ APOER2 effect, $F_{(2,59)} = 97.48$, $p < 0.0001$
3C	One-way ANOVA[a]	5	$F_{(2,25)} = 1.263$, $p = 0.3002$
3D	One-way ANOVA[a]	2	$F_{(2,3)} = 0.1782$, $p = 0.8450$
4B	One-way ANOVA[b]	8	$F_{(3,30)} = 97.57$, $p < 0.0001$
4C	One-way ANOVA[b]	6	$F_{(6,74)} = 53.92$, $p < 0.0001$
4D	One-way ANOVA[b]	12	$F_{(2,41)} = 129.4$, $p < 0.0001$
5A	One-way ANOVA[a]	8	$F_{(10,77)} = 6.086$, $p < 0.0001$
5B	One-way ANOVA[a]	3	$F_{(10,34)} = 3.635$, $p = 0.0023$
5C	One-way ANOVA[a]	3	$F_{(10,21)} = 10.42$, $p = 0.0001$
5F	Unpaired t test	6	APOER2-FL, $t_{(11)} = 2.207$, $p = 0.495$ Δ5-8, $t_{(11)} = 2.775$, $p = 0.0181$; Δ4-6, $t_{(10)} = 2.609$, $p = 0.0261$
5G	One-way ANOVA[b]	3	$F_{(11,32)} = 2.886$, $p = 0.0095$
6C	Two-way ANOVA[a]	3	$F_{(6,28)} = 23.05$, $p < 0.0001$ APOER2 effect, $F_{(3,28)} = 256.4$, $p < 0.0001$ APOE effect, $F_{(2,28)} = 293.5$, $p < 0.0001$
6E	Two-way ANOVA[b]	5	$F_{(2,44)} = 1.587$, $p = 0.2160$ APOE effect, $F_{(1,44)} = 135.3$, $p < 0.0001$ APOER2 effect, $F_{(2,44)} = 13.1$, $p < 0.0001$
6G,I	Two-way ANOVA[a]	2	$F_{(14,63)} = 2.185$, $p = 0.0182$ Time effect, $F_{(7,63)} = 36.52$, $p < 0.0001$ APOER2 effect, $F_{(2,63)} = 8.495$, $p = 0.0005$
7C	One-way ANOVA[b]	4	$F_{(4,33)} = 12.38$, $p < 0.0001$
7D	One-way ANOVA[b]	6	$F_{(4,30)} = 0.542$, $p = 0.7061$
7F	One-way ANOVA[b]	3	$F_{(4,175)} = 37.54$, $p < 0.0001$
7G	One-way ANOVA[b]	31	$F_{(4,174)} = 2.033$, $p < 0.0001$
7H	One-way ANOVA[b]	30	$F_{(4,170)} = 33.18$, $p < 0.0001$
7J	One-way ANOVA[b]	19	$F_{(4,134)} = 12.7$, $p < 0.0001$

[a] Dunnett's multiple comparisons test.
[b] Sidak's multiple comparisons test.

creates a secreted soluble form of the receptor that can bind and sequester Reelin, acting as a dominant-negative inhibitor of APOER2 (Koch et al., 2002). Near the C-terminal, both exons 15 and 18 were commonly excluded in both the cerebral cortex and heart. Combinations of the N-terminal APOER2 clones along with full-length C-terminal domain were subsequently created to generate full-length ORFs allowing for biochemical and functional analysis such as measurement of protein stability, receptor cleavage, and synaptic activity in a variety of cell types including neuronal cells.

APOER2 splice variants display differential cleavage events

APOER2 is cleaved by extracellular metalloproteases to produce a secreted APOER2 ectodomain (APOER2-ECD) and a C-terminal fragment (APOER2-CTF; Fig. 2A; Hoe and Rebeck, 2005; von Arnim et al., 2005). The APOER2-CTF is subsequently cleaved by γ-secretase, releasing an intracellular domain (APOER2-ICD) that traffics to the nucleus and leads to transcriptional changes associated with learning and memory (Fig. 2A; Telese et al., 2015). The generation of APOER2-ICD can be blocked by γ-secretase inhibitor DAPT, which leads to APOER2-CTF accumulation. An antibody directed against the carboxyl terminus of APOER2 from COS7 cell lysates transfected with APOER2-FL detected two full-length APOER2 bands where the upper band is the mature glycosylated form, and the lower band is the immature form (Fig. 2B). In addition to the full-length receptor, a smaller proteolytic CTF is detected. When we compared APOER2-FL with the APOER2 splice variant lacking exon 18 (Δex18, lacking 59 residues) in the cytoplasmic domain, we detected a decrease in the size of the CTF, consistent with the exclusion of intracellular exon 18 (Fig. 2B). To confirm γ-secretase-dependent cleavage, we treated transfected COS7 cells with the γ-secretase inhibitor DAPT. As expected, inhibition of γ-secretase leads to accumulation of the APOER2-CTF for both APOER2-FL and APOER2 Δex18 splice variants. In addition, we treated primary murine neurons with DAPT and found an increase in Apoer2-CTF generation within 24 h confirming Apoer2 cleavage occurs in neurons (Fig. 2C).

We next sought to determine whether the diversity of APOER2 splice variants affects APOER2 cleavage events. We therefore transiently transfected individual APOER2 splice variants into COS7 cells and treated them with DAPT to evaluate APOER2-CTF generation (Fig. 2D). We found that alternative splicing of certain APOER2 exons generated different amounts of CTFs compared with APOER2-FL. The pattern was not simply based on the number of ligand-binding domains, suggesting that exclusion of certain exons may alter the tertiary structure of the receptor to make the receptor more or less accessible to cleavage and generation of CTFs. For example, the APOER2 splice variant lacking exons 5–8 (Δex5–8) showed high levels of CTF generation, 215% of APOER2-FL levels, whereas APOER2 splice variants Δex5, Δex4–5, and Δex4–6 generated lower CTF levels compared with APOER2-FL (decreased by 47, 55, and 65%, respectively). We did not detect any changes in full-length APOER2 bands, including both the mature glycosylated form and immature form following DAPT treatment for any of the APOER2 variants (Fig. 2E).

APOER2 splice variants influence receptor processing

To further characterize how splicing of APOER2 influences receptor cleavage, we examined APOER2 Δex5–8 and Δex4–6, which generated the highest and lowest amounts of CTF generation, respectively, compared with APOER2-FL. We measured CTF generation in transfected COS7 cells in response to DAPT (Fig. 3A). All APOER2 variants demonstrated an increase in CTF response to increasing concentration of DAPT. However, APOER2 Δex5–8 consistently had a twofold higher CTF generation compared with APOER2-FL as opposed to Δex4–6, which showed at least twofold lower levels of CTF generation (Fig. 3B). We did not observe any changes in the amount of the glycosylated form over the immature form of APOER2 Δex5–8 and Δex4–6 (Fig. 3C).

To exclude the possibility that altered CTF generation of APOER2 Δex5–8 and Δex4–6 could arise from impaired transit

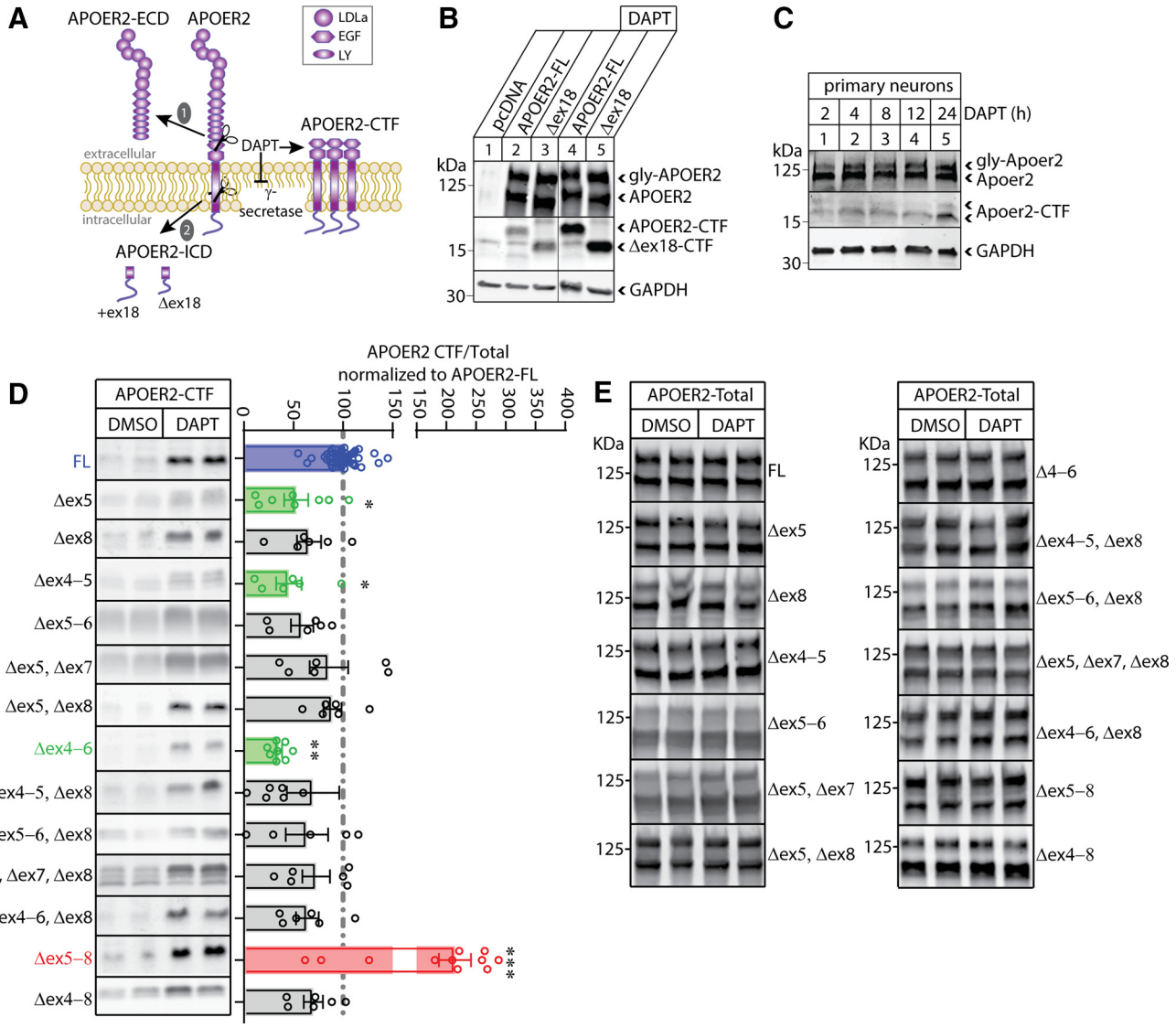

Figure 2. Proteolytic cleavage of APOER2 splice variants. ***A***, Schematic of APOER2 cleavage. APOER2 is first cleaved by an extracellular protease (1), generating a soluble ectodomain (APOER2-ECD) and a C-terminal fragment (APOER2-CTF), and (2) γ-secretase cleaves to generate intracellular domain (APOER2-ICD). The generation of APOER2-ICD can be blocked by γ-secretase inhibitor DAPT. Inclusion and exclusion of exon 18 in APOER2 will produce different sizes of APOER2-CTF and ICD. ***B***, APOER2 is cleaved by γ-secretase and generates a CTF that is shortened by splicing of exon 18 (Δex18). COS7 cells were transfected with APOER2-FL (lanes 2, 4) or APOER2-Δex18 (lanes 3, 5) and incubated with 0.001% DMSO control or the γ-secretase inhibitor DAPT at 25 μM for 24 h (lanes 4, 5). Representative immunoblots show results using a C-terminal rabbit anti-APOER2 antibody. Top, Blot displays the full-length forms where the top band indicates the glycosylated (Gly) form, and the lower band indicates the immature form of APOER2. Bottom, Blot shows APOER2-CTF where Δex18 has a lower molecular weight because of the deletion of exon 18. ***C***, APOER2-CTF detected in murine neurons and accumulates within 24 h following γ-secretase inhibitor treatment. Primary murine cortical neurons at 14 DIV were treated with 25 μM DAPT for 2, 4, 8, 12, or 24 h. GAPDH served as a loading control. ***D***, COS7 cells were transiently transfected with APOER2 splice variants and treated with either 0.0004% DMSO as control or 1 μM DAPT for 24 h. Cell lysates were blotted using the C-terminal rabbit anti-APOER2 antibody to detect both full-length and CTF fragments of APOER2. Shown are immunoblots and quantification of APOER2-CTF, which is normalized to each APOER2 variant (total, shown in ***E***), and then normalized against APOER2-FL. APOER2 Δex5–8 (red) displayed an increase in CTF generation following DAPT treatment compared with APOER2-FL (blue; $^{***}p = 0.0001$). In contrast, APOER2 Δex5, Δex4–5, and Δex4–6 (green) showed lower CTF generation ($^{*}p = 0.0278$, $^{*}p = 0.0231$, $^{**}p = 0.0007$, respectively). Quantifications were based on $n = 3$ independent transfections, and data represent mean ± SEM, and statistical significance was evaluated using one-way ANOVA with Dunnett's multiple comparisons test. For complete statistical analyses, see Table 6 and Extended Data Figure 2-1. ***E***, Both columns represent immunoblots of full-length APOER2 splice variants displaying both the glycosylated and full-length immature form of APOER2.

of APOER2 to the cell surface, we measured cell surface APOER2 by surface biotinylation. COS7 cells were transfected with APOER2-FL, Δex5–8, or Δex4–6 and incubated with sulfo-NHS-LC-Biotin to label cell-surface proteins. Biotinylated surface proteins were then precipitated and immunoblotted for APOER2. We detected only the upper mature glycosylated form and found no difference in surface glycosylated APOER2 for both Δex5–8 and Δex4–6 compared with APOER2-FL, indicating that surface expression is similar among these isoforms (Fig. 3*D*,*E*).

To verify that the changes we observed in COS7 cells reflect similar changes in neurons, we cultured neurons from newborn *Apoer2* knock-out mice and infected neurons with lentivirus that encodes human APOER2-FL, Δex5–8, or Δex4–6 at 2 DIV. At 14 DIV, neurons were treated with DAPT for 24 h and CTF levels were measured. APOER2 Δex5–8 showed higher CTF generation compared with both APOER2-FL and Δex4–6, suggesting that splicing of APOER2 influences receptor processing similarly in neurons (Fig. 3*F*).

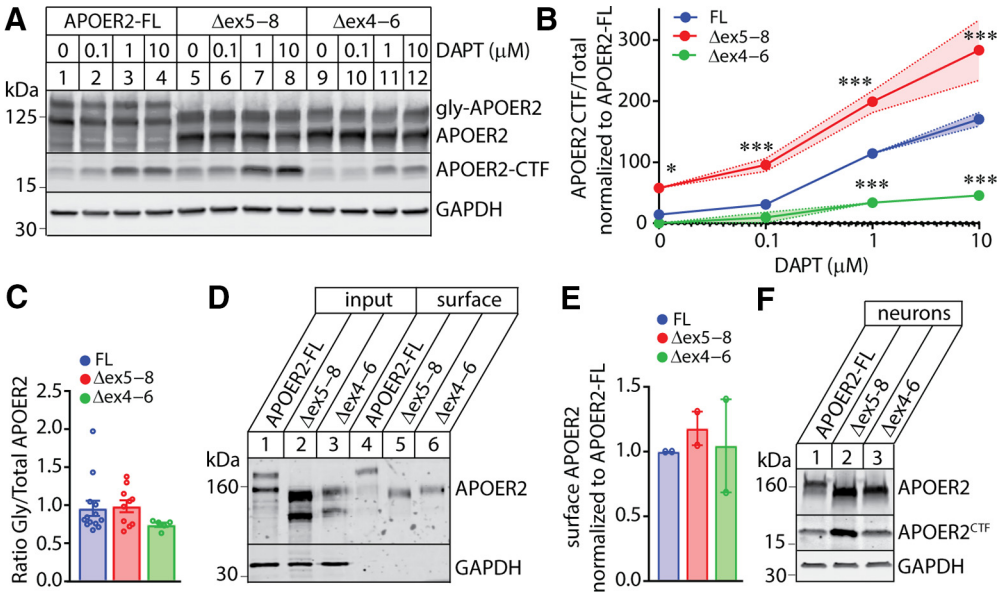

Figure 3. Splicing of APOER2 leads to differential CTF generation in COS7 cells. ***A***, ***B***, Representative immunoblots and quantitative analysis showing COS7 cells transfected with APOER2-FL, Δex5–8, or Δex4–6 and treated with 0.004% DMSO or an increasing concentration of DAPT, up to 10 μM. GAPDH served as a loading control (***A***). The graph shows the quantification of APOER2-CTF levels over total APOER2 and normalized to APOER2-FL (***B***). APOER2 Δex5–8 (red) displayed higher CTF generation compared with APOER2-FL (blue; $^{*}p = 0.0181$ at 0 μM, $^{***}p = 0.0007$ at 0.1 μM, $^{***}p = 0.0001$ at 1 and 10 μM). Conversely, APOER2 Δex4–6 (green) showed lower levels of CTF generation compared with APOER2-FL; $^{***}p = 0.0001$ at 1 and 10 μM. Quantifications are based on $n = 3$ independent transfections, and data with error envelope represent mean ± SEM. ***C***, Graph shows the quantification of the ratio of glycosylated band over total APOER2 expressed. $N = 3$ independent transfections. ***D***, ***E***, Representative immunoblots and quantification analysis from two independent transfections showing COS7 cells transfected with APOER2-FL, Δex5–8, or Δex4–6 and surface biotinylated. Precipitated proteins (lanes 4–6) and total input lysates (lanes 1–3) were immunoblotted for APOER2, and the amount of glycosylated surface APOER2 was taken as the measure of band intensity against input and normalizing to APOER2-FL. $N = 2$ independent transfections. ***F***, Primary mouse *Apoer2* knock-out cortical neurons were infected with lentivirus that expressed human APOER2-FL, Δex5–8, or Δex4–6 and treated with 25 μM DAPT for 24 h. Immunoblots show that APOER2 Δex5–8 showed higher CTF generation compared with APOER2-FL. GAPDH served as loading control. All data represent mean ± SEM, and statistical significance was evaluated using one-way ANOVA with Dunnett's multiple comparisons test. For complete statistical analyses, see Table 6 and Extended Data Figure 3-1.

APOER2 splice variants regulate proteolytic release of APOER2-ICD

Previous studies suggested that γ-secretase-dependent release of APOER2-ICD functions in transcriptional regulation (Telese et al., 2015). Because APOER2 Δex5–8 and Δex4–6 showed differential CTF generation, we wanted to test whether CTF changes alter transcriptional activation mediated by APOER2 as an indirect measure for APOER2 cleavage. We therefore inserted Gal4-VP16 domain at the cytoplasmic boundary of the APOER2 transmembrane region. Gal4-VP16 is a fusion of the yeast Gal4 DNA binding protein with VP16 that serves as the viral transcriptional activator (Sadowski et al., 1988; Biederer et al., 2002). This allows for transactivation independent of potentially necessary transcriptional coactivators while still requiring APOER2 cleavage and the translocation of the APOER2-ICD into the nucleus (Fig. 4*A*). We transfected the APOER2-Gal4/VP16 fusion protein into COS7 cells and measured transactivation from a cotransfected Gal4-dependent reporter plasmid that encodes luciferase. In addition, cells were cotransfected with a constitutive β-galactosidase expression vector to control for transfection efficiency. Transfection of APOER2-FL-Gal4/VP16 transactivated Gal4-dependent transcription by 309%, suggesting APOER2 was cleaved and the APOER2-ICD released (Fig. 4*B*). When we transfected the APOER2 Δex5–8-Gal4/VP16 construct, the reporter luciferase activity was increased 2.8-fold over APOER2-FL, an even more potent transactivator compared with APOER2-FL. In contrast, APOER2 Δex4–6 showed twofold lowered luciferase activity compared with APOER2-FL suggesting APOER2 splice isoforms play an important role in modulating APOER2-ICD transactivation.

To confirm APOER2-ICD generation is γ-secretase-dependent and contributes to the increase in reporter luciferase activity, we treated transfected COS7 cells with DAPT, which blocks APOER2-ICD generation. Blocking γ-secretase activity decreased the reporter luciferase activity for APOER2-FL, Δex5–8, and Δex4–6 variants (Fig. 4*C*). As a positive control for the transactivation assay, we tested APP, which has been shown to robustly activate the reporter luciferase activity and is sensitive to DAPT treatment. (Fig. 4*D*; Cao and Südhof, 2001).

Mint1 adaptor protein promotes APOER2-Gal4 transactivation

The C terminus of APOER2 has been shown to bind to several cytosolic adaptor proteins such as Dab, JIP, Fe65, and Mint proteins (Gotthardt et al., 2000; Stockinger et al., 2000; Hoe et al., 2006; He et al., 2007). To determine whether any of these adaptor proteins affect APOER2 cleavage and signaling, we used the transactivation assay, where we only introduced Gal4 into the cytoplasmic tail for APOER2-FL, Δex5–8, and Δex4–6 variants to study the effects of several adaptor proteins including Dab1, Dab2, JIP1, JIP2, Mint1, Mint2, and Fe65 on APOER2 cleavage. Mint1 was the only adaptor protein that enhanced transactivation of APOER2-FL (1.8-fold), and Δex5–8 (1.4-fold) compared with Gal4 alone (Fig. 5*A*,*B*). Meanwhile, Dab2 and both Mints 1 and 2 increased transactivation of APOER2 Δex4–6, by 1.5-, 2.1-, and 1.7-fold, respectively (Fig. 5*C*). PSD95 has been shown to bind intracellularly to APOER2 and affect synaptic plasticity but had no effect on transactivation for APOER2-FL, Δex5–8, and Δex4–6 variants.

Because APOER2-FL has been shown to bind Mint1 (Minami et al., 2010), we wanted to examine whether the APOER2 variants also bind Mint1 as efficiently as APOER2-FL. We cotransfected COS7 cells with pcDNA, APOER2-FL, Δex5–8, or Δex4–6 variant and GFP-Mint1. We immunoprecipitated with GFP and immunoblotted for APOER2 and found all three APOER2 variants coprecipitated with Mint1 (Fig. 5*D*). Western blot analysis confirmed that the levels of total APOER2 and Mint1 were consistent across transfections (indicated by input blots).

We next examined whether Mint1 affects CTF generation of APOER2 variants. We cotransfected APOER2-FL, Δex5–8, or Δex4–6 variant with either GFP or GFP-Mint1 and consistently found Mint1 increased APOER2 protein levels for all three variants compared with GFP control, suggesting Mint1 affects APOER2 protein stability (Fig. 5*E*,*F*). The apparent increase in abundance of APOER2 protein induced by Mint1 expression is consistent with APOER2 Δex5–8 having higher CTF generation compared with APOER2-FL and increased in response to DAPT (Fig. 5*G*).

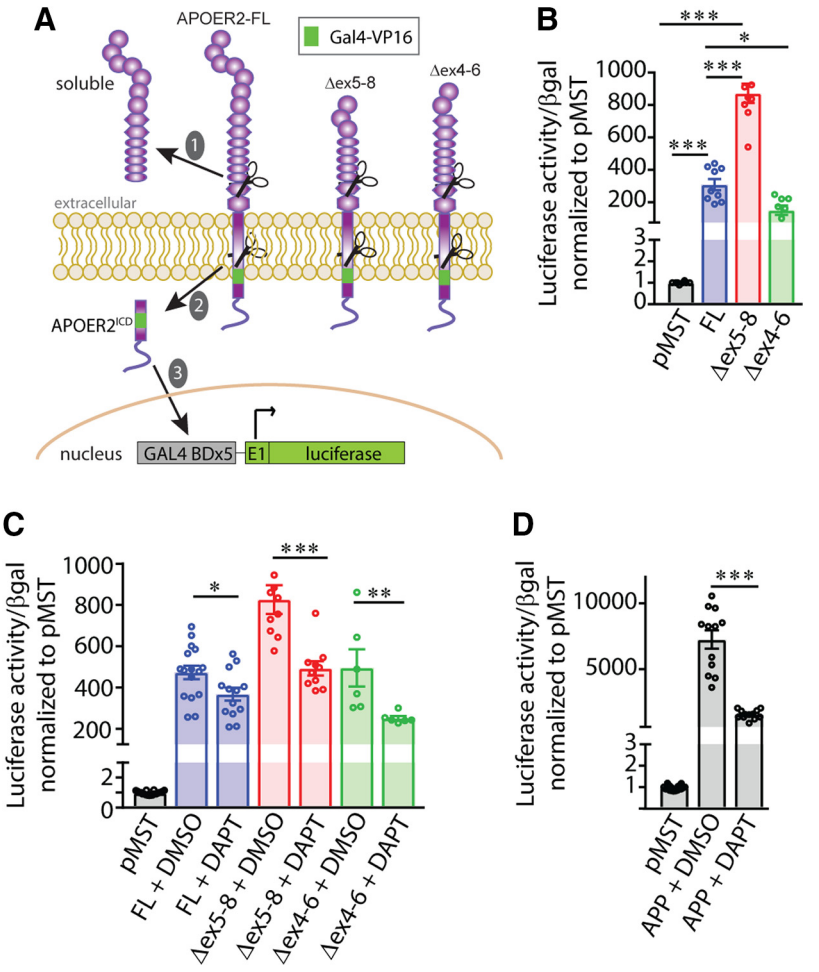

Figure 4. APOER2 splice variants display differential transcriptional activation. ***A***, Constructs for the transactivation assay were generated with the Gal4/VP16 domain (green) inserted at the cytoplasmic boundary of the APOER2 transmembrane region. ***B***, APOER2-Gal4/VP16 fusion constructs were cotransfected into COS7 cells along with a Gal4-dependent luciferase reporter plasmid and a β-galactosidase plasmid (control for transfection efficiency); pMst alone was used as a negative control. For quantification, luciferase activity was normalized to β-gal activity and calculated relative to the cells expressing pMst alone. APOER2 Δex5-8 showed an increase in transactivation compared with APOER2-FL, $^{***}p < 0.0001$; whereas Δex4-6 showed a decrease in transactivation compared with APOER2-FL, $^{*}p = 0.0361$. $N = 3$ independent transfections. ***C***, APOER2 splice variants transcriptional activity is dependent on γ-secretase. APOER2-Gal4/VP16 fusion constructs were cotransfected into COS7 cells along with a Gal4-dependent luciferase reporter plasmid and a β-galactosidase plasmid and treated with either 0.001% DMSO or 25 μM of DAPT for 24 h. DAPT treatment reduces transactivation compared with DMSO control for APOER2-FL, $^{*}p = 0.0297$; Δex5–8, $^{***}p < 0.0001$; and Δex4–6, $^{**}p = 0.0028$, based on $n = 3$ independent transfections. ***D,*** Graph represents the quantification for APP transactivation that is dependent on γ-secretase, which serves as a positive control for the transactivation assay. DAPT treatment inhibits APP-ICD transactivation; $^{***}p < 0.0001$, $n = 3$ independent transfections. All data represent mean ± SEM, and statistical significance was evaluated by a one-way ANOVA with Sidak's multiple comparisons test. For complete statistical analyses, see Table 6 and Extended Data Figure 4-1.

Mimetic APOE peptide influences APOER2 splice variant receptor processing

Previous studies have demonstrated that mouse Apoer2 cleavage by γ-secretase can be induced in a ligand-regulated manner by both Reelin and APOE (Hoe and Rebeck, 2005; Telese et al., 2015). To determine whether APOE affects APOER2 splice variant cleavage, we took advantage of a short 17 amino acid APOE mimetic peptide (133–149 residues), also known as COG-133, derived from the receptor-binding region (Laskowitz et al., 2001; Fig. 6*A*). The APOE mimetic peptide binds to LDLR and has been validated in multiple *in vitro*, *in vivo*, and clinical applications (Lynch et al., 2003; Azevedo et al., 2012; Vitek et al., 2012; Latypova et al., 2014; White et al., 2014). In addition, the APOE mimetic peptide excludes the amino acid positions that vary between APOE isoforms (at position 112, 158) and the lipid-binding domain (244–272 residues), making it a pan-APOE peptide (Fig. 6*A*). COS7 cells were transfected with individual APOER-FL, Δex5–8, or Δex4–6 variants and pretreated with a low dosage of 0.1 μM DAPT for 24 h. At 48 h, transfected cells were treated with an increasing amount of APOE mimetic peptide ranging from 5 to 50 μM for 30 min. Cell lysates were collected and processed for detection of APOER2-CTFs. APOER2 Δex5–8 generated a twofold higher CTF generation compared with APOER2-FL and consistently increased in response to the increasing concentration of APOE peptide (Fig. 6*B*–*D*). In contrast, Δex4–6 showed 1.6-fold lowered levels of CTF generation compared with APOER2-FL (Fig. 6*B*–*D*). APOE mimetic peptide induced the most pronounced increase in CTF generation at 50 μM for all three APOER2 variants compared with each corresponding vehicle treatment (fourfold for APOER2-FL, 2.4-fold for Δex5–8, and 3.2-fold for Δex4–6; Fig. 6*E*). We also evaluated the time course of the APOE peptide effects on APOER2-CTF generation and found 30 min to 3 h was the optimal time of APOER2-CTF generation with Δex5–8 having a 1.3-fold increase compared with APOER2-FL. By 12 h, the APOE mimetic peptide had no effects on APOER2-CTF generation (Fig. 6*F*–*I*). We did not detect any changes between APOER2-FL and Δex4–6 isoform (Fig. 6*I*).

APOER2 splice variants have differential synaptic properties

It has been well established that mouse Apoer2 mediates synaptic signaling through both presynaptic and postsynaptic mechanisms (Beffert et al., 2005; Qiu et al., 2006; Bal et al., 2013).

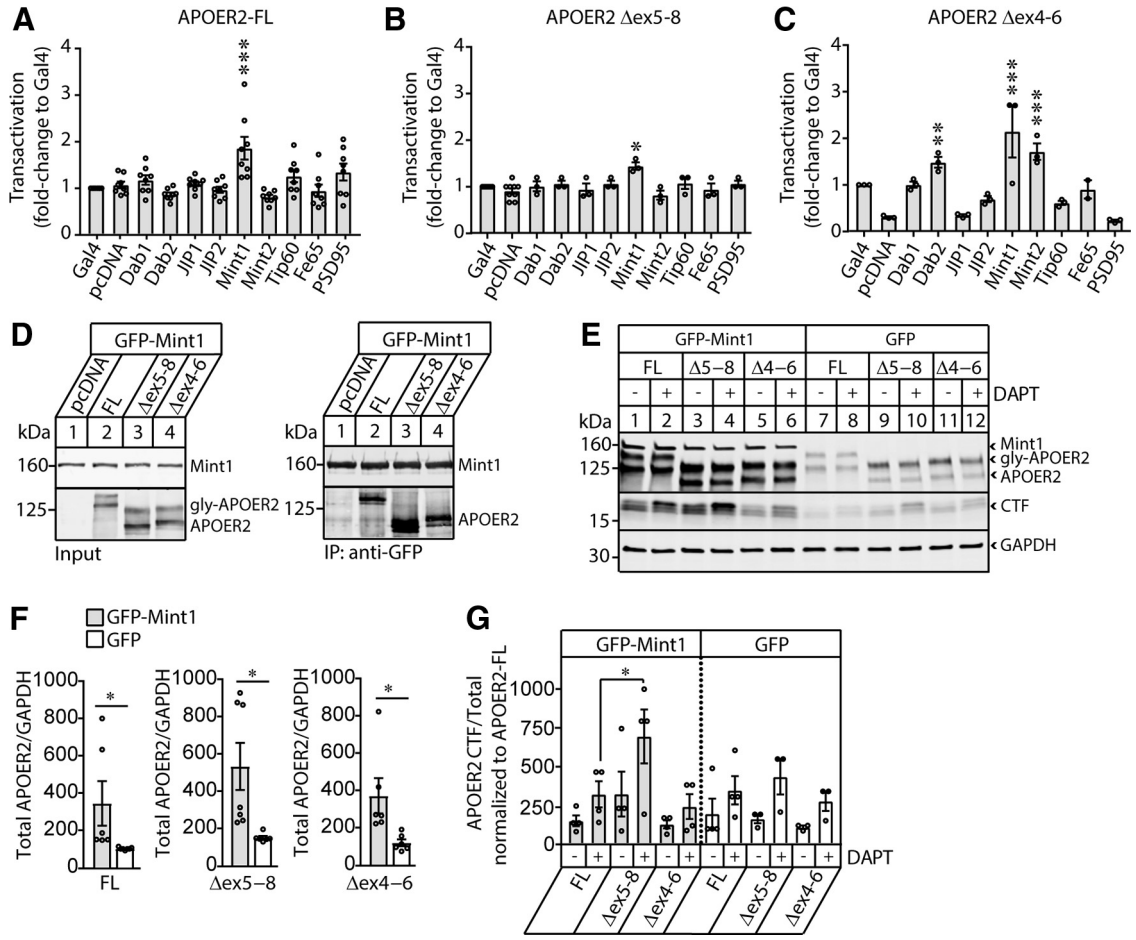

Figure 5. Adaptor protein screen reveals Mint1 as the main cytosolic adaptor protein mediating APOER2 transactivation. ***A–C***, COS7 cells were transiently cotransfected with pMst-Gal4-APOER2-FL (***A***), pMst–Gal4–Δex5–8 (***B***), or pMst–Gal4–Δex4–6 (***C***) plasmids along with Gal4-luciferase reporter plasmid, a β galactosidase plasmid, and the various adaptor protein plasmids as indicated in the labels (bottom). Transactivation is shown as the fold change compared with Gal4 alone. Mint1 enhanced transactivation of APOER2-FL and Δex5–8 (***$p = 0.0001$). Meanwhile, Dab2 and both Mints 1 and 2 increased transactivation of APOER2 Δex4–6 (**$p = 0.0022$, ***$p = 0.0001$, Mint1; and ***$p = 0.0003$, Mint2; $n = 3$ independent transfections). Data represent mean ± SEM, and statistical significance was evaluated using one-way ANOVA with Dunnett's multiple comparisons test. ***D***, All three APOER2 splice variants coimmunoprecipitate with Mint1 protein. COS7 cells were cotransfected with pcDNA, APOER2-FL, Δex5–8, or Δex4–6 variant and GFP-Mint1. Cell lysates were immunoprecipitated with anti-GFP and immunoblotted with anti-APOER2 and anti-GFP antibody (right), input (left). ***E***, Mint1 stabilizes APOER2 protein levels. COS7 cells were cotransfected with APOER2-FL, Δex5–8, or Δex4–6 variant with either GFP or GFP-Mint1 (indicated across top). Cells were treated with either 0.00,004% DMSO as vehicle control or 0.1 μM DAPT and immunoblotted for anti-GFP to detect Mint1 and anti-APOER2. GAPDH serves as loading control. ***F***, Quantification of total APOER2 from ***E*** shows an increase in total APOER2 levels in the presence of Mint1 across all three APOER2 splice variants with $n = 3$ independent transfections; *$p = 0.0495$, APOER2-FL; *$p = 0.0181$, Δex5–8; *$p = 0.0261$, Δex4–6. Data represent mean ± SEM, and statistical significance was evaluated using two-tailed unpaired t test. ***G***, Quantification of APOER2-CTF levels from ***E***. $N = 3$ independent transfections. Data represent mean ± SEM, and statistical significance was evaluated by a one-way ANOVA with Sidak's multiple comparisons test where *$p = 0.0325$. For complete statistical analyses, see Table 6 and Extended Data Figure 5-1.

However, the functional role of human APOER2 splice variants on synaptic transmission is largely unexplored. We cultured hippocampal neurons from *Apoer2* heterozygous and homozygous knock-out mice individually. To examine the synaptic properties of human APOER2 splice variants, we infected *Apoer2* knock-out neurons with lentiviral human untagged APOER2-FL, Δex5–8, or Δex4–6 at 2 DIV and performed whole-cell recordings starting at 14 DIV. We verified APOER2 protein expression in *Apoer2* knock-out neurons rescued with APOER2-FL, Δex5–8, or Δex4–6 lentivirus (Fig. 7*A*). To monitor the frequency and amplitude of spontaneous postsynaptic currents, neurons were treated with TTX to block action potentials. Loss of *Apoer2* decreased miniature event frequency by 76% but not amplitude in excitatory synapses compared with *Apoer2* heterozygous neurons (Fig. 7*B–D*). This selective deficit in mEPSC frequency suggests that loss of *Apoer2* may alter presynaptic release probability. We next tested whether expression of lentiviral human APOER2-FL, Δex5–8, or Δex4–6 rescued the effects of *Apoer2* knock-out neurons on mEPSCs. We found APOER2-FL restored the miniature event frequency in excitatory synapses, inducing a nearly twofold increase compared with *Apoer2* heterozygous neurons, but Δex5–8 did not rescue miniature event frequency. In addition, Δex4–6 restored the miniature event frequency similar to *Apoer2* heterozygous neurons.

We next examined whether the decrease in spontaneous neurotransmission in *Apoer2* knock-out neurons and Δex5–8 infected neurons are because of changes in the number of synapses. We, therefore performed immunofluorescence labeling using antibodies against the presynaptic protein synapsin and the postsynaptic marker PSD95 on *Apoer2* knockout neurons rescued with lentiviral human APOER2-FL, Δex5–8, or Δex4–6 at 14 DIV. We measured the number of synapsin and PSD95 puncta independently and the number of synapses defined by the colocalization of synapsin and PSD95 (Fig. 7*E*). *Apoer2* knock-out neurons decreased the number of synapsin puncta by 56% compared with *Apoer2* heterozygous neurons. Human APOER2-FL lentivirus rescued the *Apoer2* knock-out phenotype similar to

Apoer2 heterozygous neurons. However, Δex5–8 infected neurons had a 18% decrease in the number of synapsin puncta compared with APOER2-FL (Fig. 7*F*). We also found a similar 20% decrease in the number of PSD95 puncta in neurons infected with Δex5–8 lentivirus compared with APOER2-FL (Fig. 7*G*). Loss of *Apoer2* led to a 35% decrease in the total number of synapses compared with *Apoer2* heterozygous neurons, which was rescued by APOER2-FL lentivirus (Fig. 7*H*). APOER2 Δex5–8 consistently had a 20% reduction in the number of synapses compared with APOER2-FL.

In addition, we immunostained with the presynaptic marker VAMP2, a protein essential in synaptic vesicle fusion process (Fig. 7*I*). We found a 30% reduction in VAMP2 puncta in *Apoer2* knock-out neurons compared with *Apoer2* heterozygous neurons. Lentiviral infection of human APOER2-FL rescued the decrease in VAMP2 puncta of *Apoer2* knock-out neurons. However, Δex5–8 infected neurons decreased in the number of VAMP2 puncta by 19% compared with APOER2-FL (Fig. 7*J*). Overall, these results suggest that the decrease in the total number of synapses and/or VAMP2 may contribute to the decrease in miniature event frequency found in *Apoer2* knock-out neurons and Δex5–8 infected neurons.

Discussion

In this study, we identified a number of distinct in-frame human APOER2 isoforms from the cerebral cortex that arise from exon-skipping events, generating a large portfolio of APOER2 splice variants with differing combinations of ligand-binding repeats. The majority of the individual exon–exon junctions identified within ORFs corresponded to junctions curated in databases such as GTEx (GTEx Consortium, 2015) and the National Center for Biotechnology Information, suggesting that most clones in our collection were derived from genuine splicing events. For example, we detected the same junctions associated with skipping of exons 5, 15, and 18. Less than 1% of sequenced PCR products led to nonsense mediated decay. We found APOER2-FL is a predominant isoform in human brain, with similar percentages to the isoform lacking exon 5 (Δex5) and another lacking exon 5 in combination with exon 8. Exon 5 skipping in APOER2 is a common event and occurs in combination with many other skipped exons, with 79% of brain transcripts lacking exon 5 alone or in combination with other skipped exons. Importantly, the vast majority of the skipped exons led to in-frame transcripts because of the shared codon phase in all the ligand-binding domains and first two EGF repeats. As the increased diversity of isoforms occurs primarily in the ligand-binding regions of APOER2, we propose splicing of APOER2 can alter the binding profile for critical ligands to

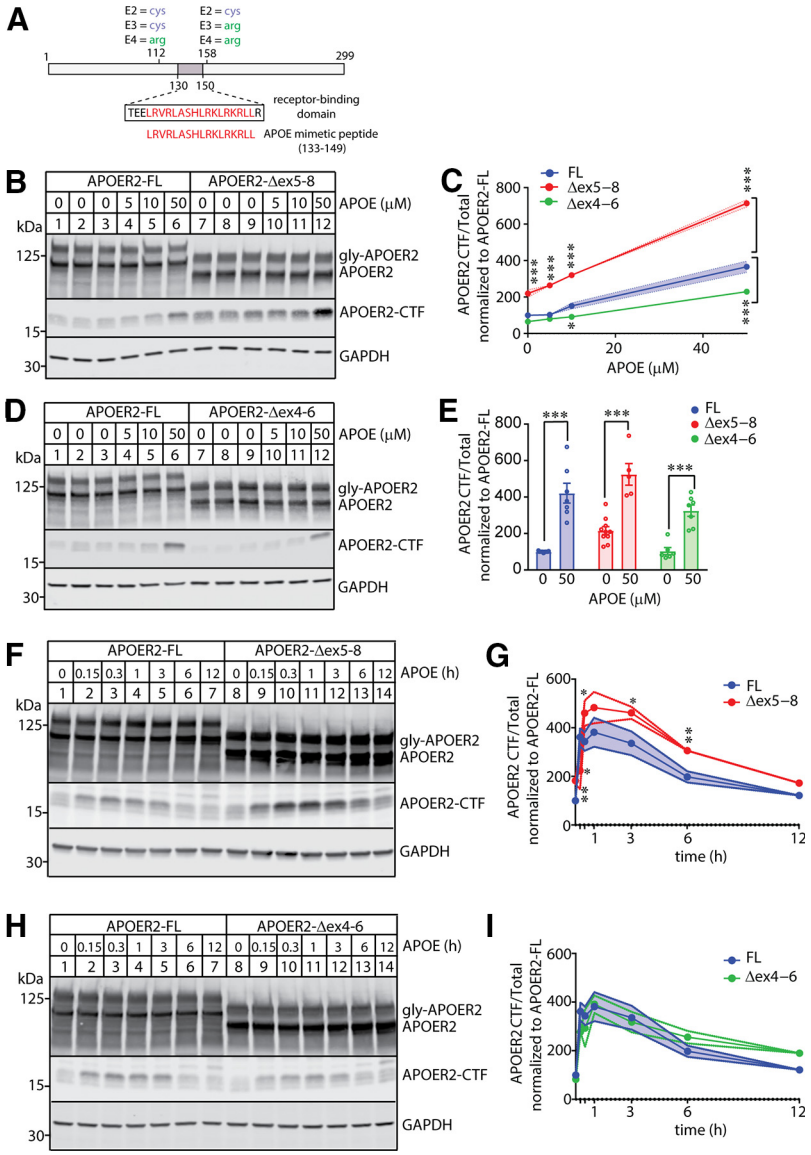

Figure 6. Mimetic APOE peptide induces APOER2 splice variant processing. ***A***, Schematic of APOE and APOE mimetic peptide (in red, 133–149 residues) within the receptor binding domain. APOE isoforms (E2, E3, and E4) lies outside the APOE mimetic peptide at positions 112 and 158. ***B–D***, Representative immunoblots and quantitative analysis of COS7 cell lysates that was transfected with APOER2-FL (***B***, ***D***), Δex5–8 (***B***) or Δex4–6 (***D***), treated with 0.00,004% DMSO or low 0.1 μM DAPT for 24 h followed by increasing concentration of APOE mimetic peptide. Quantification showing APOER2 Δex5–8 (red) had higher CTF generation compared with APOER2-FL (blue) at all concentrations (***C***); ***$p = 0.0001$. Conversely, APOER2 Δex4–6 (green) showed lower CTF generation compared with APOER2-FL at 10 μM (*$p = 0.0172$) and 50 μM (***$p = 0.0001$). $N = 3$ independent transfections. Data represent mean ± SEM, and statistical significance was evaluated by a one-way ANOVA with Dunnett's multiple comparisons test. ***E***, Graph shows induction of APOER2-CTF generation across APOER2-FL, Δex5–8, and Δex4–6 at 50 μM of mimetic APOE peptide treatment; *** $p < 0.0001$. $N = 3$ independent transfections. Data represent mean ± SEM, and statistical significance was evaluated by a one-way ANOVA with Sidak's multiple comparisons test. ***F–I***, Representative immunoblots and quantitative analysis of COS7 cell lysates that was transfected with APOER2-FL (***F***, ***H***), Δex5–8 (***F***, ***G***) or Δex4–6 (***H***, ***I***), treated with 0.00,004% DMSO or low 0.1 μM DAPT for 24 h followed by treatment followed by 50 μM APOE mimetic peptide at multiple time points starting at 15 min to 12 h. Data represent mean ± SEM. APOER2 Δex5–8 had a greater effect compared with APOER2-FL (**$p = 0.0091$ at 0 min, *$p = 0.0149$ at 15 min, *$p = 0.0298$ at 30 min, *$p = 0.0279$ at 3 h, **$p = 0.0061$ at 6 h with $n = 2$ independent transfections). By 12 h, the APOE mimetic peptide had no effects on APOER2-CTF generation. Data represent mean ± SEM, and statistical significance was evaluated using one-way ANOVA with Dunnett's multiple comparisons test. For complete statistical analyses, see Table 6 and Extended Data Figure 6-1.

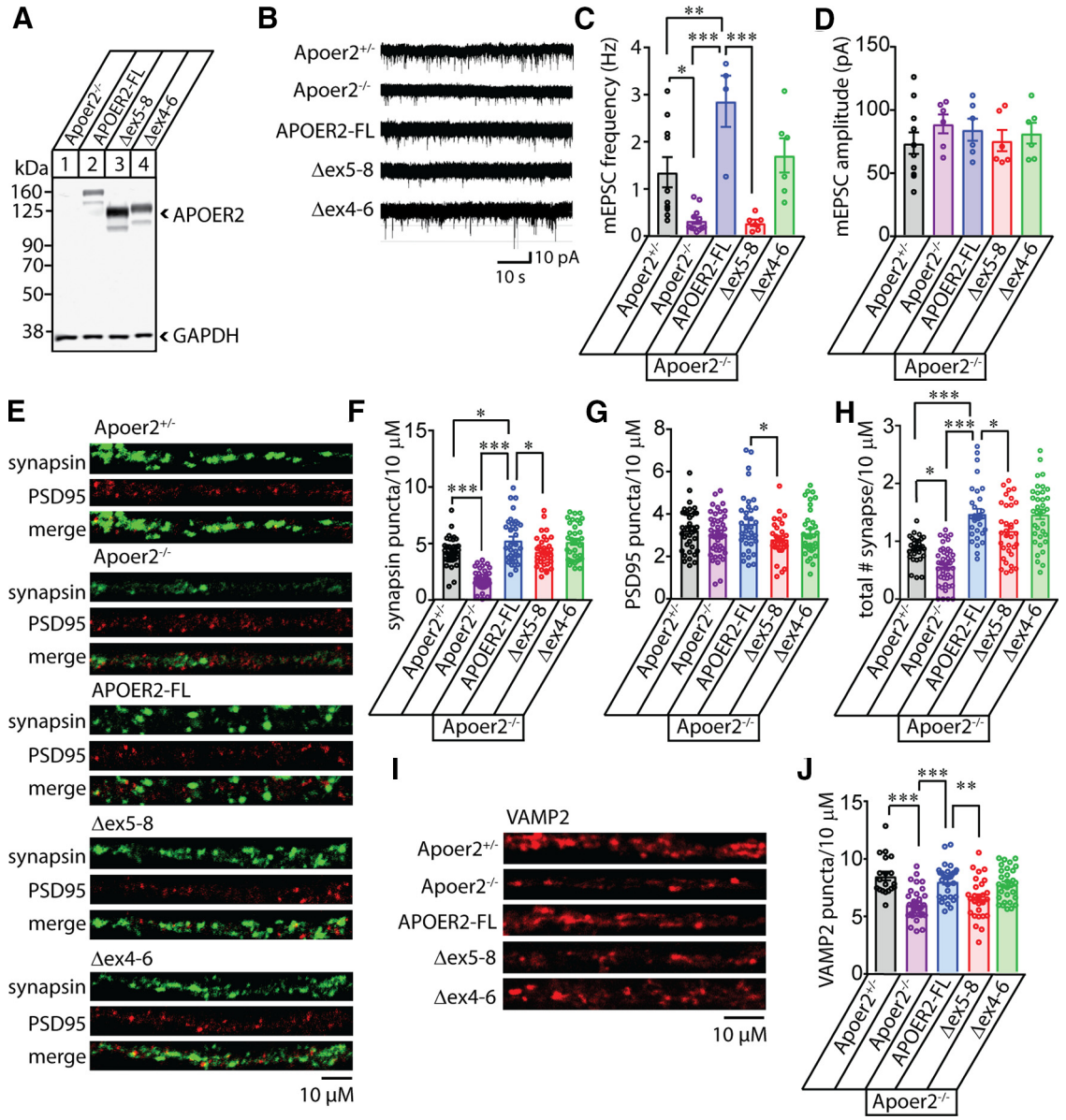

Figure 7. Mouse *Apoer2* knock-out neurons show reduced spontaneous synaptic transmission that can be rescued by human APOER2-FL. ***A***, Representative immunoblot showing neuronal lysates isolated from primary murine neuronal cultures of *Apoer2* knock-out cortices (lane 1) that were infected with human APOER2-FL (lane 2), Δex5–8 (lane 3), or Δex4–6 (lane 4) lentivirus using a rabbit anti-APOER2 C-terminal antibody. GAPDH served as a loading control. ***B***, Sample traces showing miniature excitatory postsynaptic current (mEPSC) for *Apoer2* heterozygous and homozygous knockout hippocampal neurons at 14–17 DIV. *Apoer2* knock-out neurons were infected with human APOER2-FL, Δex5–8, or Δex4–6 lentivirus. ***C***, ***D***, Bar graphs of quantification revealed a decrease in miniature frequency but not amplitude in *Apoer2* knockout neurons compared with heterozygous neurons, $*p = 0.012$. Addition of lentiviral expressing APOER2-FL to *Apoer2* knock-out neurons rescues the frequency ($***p < 0.0001$), and increased mEPSC compared with *Apoer2* heterozygous neurons ($**p = 0.007$) but not Δex5–8. There was a decrease in mEPSC when we compared Δex5–8 to APOER2-FL, $***p < 0.0001$. $N = 5$ independent neuronal cultures. ***E***, Hippocampal neuronal processes of *Apoer2* heterozygous and homozygous knock-out neurons. *Apoer2* knock-out neurons were infected with human APOER2-FL, Δex5–8, or Δex4–6 lentivirus stained with synapsin (green) and PSD95 (red) at 14 DIV. Scale bar, 10 μm. ***F***, Bar graph of quantification revealed a decrease in the number of synapsin puncta in *Apoer2* knockout neurons compared with *Apoer2* heterozygous neurons, $***p < 0.0001$. Infection of human APOER2-FL rescues the *Apoer2* knockout phenotype, $***p < 0.0001$, and increased in synapsin puncta compared with *Apoer2* heterozygous neurons, $*p = 0.0237$. There was a decrease in synapsin puncta when we compared Δex5–8 with APOER2-FL, $*p = 0.023$. ***G***, Quantification of the number of PSD95 puncta showed a decrease in the number of PSD95 puncta between Δex5–8 and APOER2-FL, $*p < 0.0356$. ***H***, Quantification of synapsin and PSD95 colocalization in neuronal processes show a decrease in the number of total synapses in *Apoer2* knock-out neurons compared with heterozygous neurons, $***p < 0.0001$. Infection of human APOER2-FL rescues the *Apoer2* knock-out phenotype, $***p < 0.0001$; and increased when we compared with Apoer2 heterozygous neurons, $***p < 0.0001$. However, there was a decrease in the number of synapse when we compared Δex5–8 to APOER2-FL, $*p = 0.024$. ***I***, Hippocampal neuronal processes were stained with VAMP2 at 14 DIV. Scale bar, 10 μm. ***J***, Bar graph of quantification revealed a decrease in the number of VAMP2 puncta in *Apoer2* knock-out neurons compared with *Apoer2* heterozygous neurons, $***p < 0.0001$. Infection of human APOER2-FL rescues the *Apoer2* knock-out phenotype, $***p < 0.0001$. There was a decrease in VAMP2 puncta when we compared Δex5–8 with APOER2-FL, $**p = 0.002$. $N = 2$ independent neuronal cultures for ***E–J***. All data represent mean ± SEM, and statistical significance was evaluated by a one-way ANOVA with Sidak's multiple comparisons test. For complete statistical analyses, see Table 6 and Extended Data Figure 7-1.

regulate function (Fig. 8). In contrast, Reelin binds to exon 2 of APOER2 (D'Arcangelo et al., 1999; Yasui et al., 2010), and, interestingly, exon 2 splicing was not found in any of our screens, nor is it identified as a spliced exon on GTEX, suggesting that retention of the Reelin-APOER2 interaction is a crucial function. Another important observation is that exon skipping of APOER2 is far more common in the brain compared with the heart, suggesting an important functional

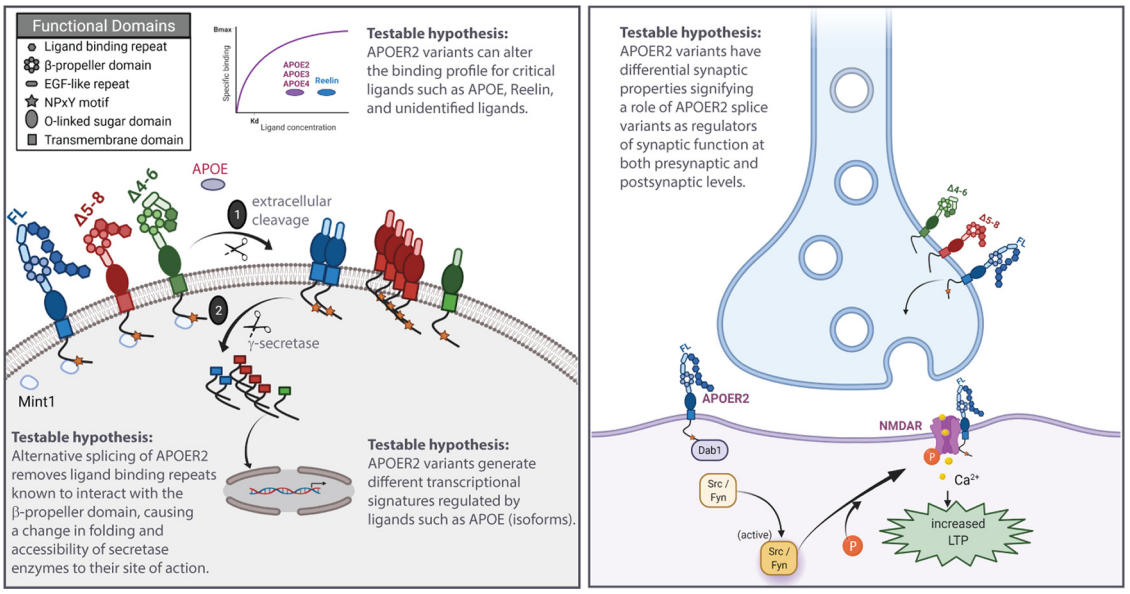

Figure 8. Model of the differential cleavage events and synaptic properties of human APOER2 isoforms. Alternative splicing of APOER2 removes ligand-binding repeats that could alter the binding profile for critical ligands such as APOE, Reelin, and unidentified ligands. Changes in APOER2 ligand-binding repeats can also modify the structural components known to interact with the β-propeller domain causing a change in folding and accessibility of secretase enzymes to their site of action. The differential cleavage events of APOER2 in turn may generate different transcriptional signatures regulated by ligands and alter synaptic properties both at the presynaptic and postsynaptic levels suggesting a role of APOER2 variants as regulators of synaptic function.

consequence of increased transcript diversity in the brain (Yeo et al., 2004).

APOER2 is cleaved by secretase enzymes, leading to CTF generation (Hoe and Rebeck, 2005; von Arnim et al., 2005). We found the length of the final protein, as determined by an increasing number of skipped exons, may not determine the accessibility to secretase enzymes and CTF generation. For example, APOER2 Δex5–8 generated the largest amount of CTF, whereas Δex4–6 generated the least amount of CTF compared with APOER2-FL. In LDLR, which shares a similar number and organization of exons as well as functional protein domains to APOER2, the ligand-binding domain folds back over the β-propeller via the calcium-binding loop (Rudenko et al., 2002). Thus, the ligand-binding domain of APOER2 may fold back toward the plasma membrane, possibly through contacts between the ligand-binding domain and the β-propeller domain. We propose that alternative splicing of APOER2 removes ligand-binding repeats known to interact with the β-propeller domain, causing a change in folding and accessibility of secretase enzymes to their site of action (Fig. 8).

APOER2 cleavage also leads to generation of an ICD that can translocate to the nucleus and alter the epigenetic signature in learning and memory transcripts that is dependent on Reelin binding (Telese et al., 2015). We verified that the changes in APOER2-CTF generation also lead to similar changes in ICD transactivation using an *in vitro* luciferase assay, where APOER2-FL led to an increase in luciferase activation. An APOER2 isoform-specific increase was observed with Δex5-8, whereas Δex4–6 had reduced transactivation relative to APOER2-FL. These results suggest that APOER2 cleavage generates both an intracellular CTF, followed by ICD generation, which can translocate to the nucleus and presumably alter transcription. Further, different APOER2 splice variants affect this process by altering the amount of CTF and ICD generated. However, the direct consequences of ICD changes on transcriptional regulation and other downstream functional signaling remain to be elucidated (Fig. 8).

Although it is clear Reelin acts as a signaling molecule by binding to APOER2 and VLDLR to activate downstream signaling pathways essential for brain development and synaptic plasticity (Trommsdorff et al., 1999; Beffert et al., 2005), not much is known regarding the functional consequences of APOE binding. APOE was originally not thought to be a signaling molecule, largely because of the high micromolar concentrations found in the brain and other tissues (Pitas et al., 1987; Mahley, 1988; Grehan et al., 2001). However, recent studies show that APOE acts as a signaling molecule via binding to LDLR, which in turn, stimulates phosphorylation of the ERK/MAPK signaling pathway (Huang et al., 2017). We posit that APOE signaling may occur through regulated surface expression of distinct APOER2 isoforms that allow neurons to finely tune and activate downstream signaling pathways. Indeed, our data show a potential role of APOE in regulating transient APOER2 cleavage that may have transcriptional regulation. As such, tight regulation of APOER2 splicing in the ECD could mediate specific interactions with APOE or other ligands. In the closely related LDLR, APOE was shown to bind to the analogous exon 5 (Fisher et al., 2004). Our results demonstrate that APOER2 splice variants (Δex5–8 and Δex4–6) missing exon 5 are capable to respond to APOE and affect APOER2 cleavage, thus suggesting APOE binding is not restricted to exon 5. The LDLa repeats within exons 2 and 3 or EGF-like repeats can certainly bind APOE, and future experiments should elucidate the specific interactions of APOE to APOER2 splice variants.

The binding of Reelin to APOER2 mediates synaptic signaling through both presynaptic and postsynaptic mechanisms (Weeber et al., 2002; Beffert et al., 2005; Chen et al., 2005; Qiu et al., 2006; Bal et al., 2013). Mouse Apoer2 is important for Reelin-induced hippocampal LTP, and LTP induction is regulated by alternative splicing of exon 19 in mouse (exon 18 in human), which encodes an intracellular domain that interacts with

postsynaptic PSD95 adaptor protein (Beffert et al., 2005). Reelin also acts presynaptically to selectively augment spontaneous neurotransmitter release, which requires an increase in presynaptic Ca^{2+} initiated by Apoer2 signaling (Bal et al., 2013). Neurons lacking *Apoer2* did not elicit a Reelin-dependent increase in spontaneous transmission (Bal et al., 2013). Similarly, we found loss of mouse *Apoer2* decreased mEPSC frequency, but not amplitude, suggesting loss of *Apoer2* may alter presynaptic neurotransmitter release. Lentiviral rescue with APOER2-FL restored the mEPSC frequency, but not Δex5–8. In addition, Δex4–6 restored the mEPSC frequency to a level similar to heterozygous *Apoer2* neurons. These results suggest that mouse Apoer2 is required for spontaneous neurotransmitter release in mature neurons, and human APOER2 splice variants have differential synaptic properties signifying a role of APOER2 splice variants as regulators of synaptic function (Fig. 8). APOER2 interaction with neuronal adaptor Mint1 (He et al., 2007) also supports a role of APOER2 in presynaptic function as knock out of Mint adaptor proteins lead to a decline in spontaneous neurotransmitter release (Ho et al., 2006).

A limitation of this study is that we amplified the N-terminal and C-terminal ORF of *APOER2* separately, which does not capture the entire APOER2 full-length transcripts. To address this in a separate study, we used long-read sequencing to map the entire *APOER2* transcript from human brain (Gallo et al., 2022). This study was an in-depth examination defining a repertoire of diverse and novel full-length *Apoer2* isoforms, where we highlighted species-specific differences in splicing decisions across the mouse and human cerebral cortex. Indeed, we confirmed both human APOER2 Δex5–8 and Δex4–6 are present in the human cerebral cortex from long-read sequencing (Gallo et al., 2022). APOER2 Δex5–8 was also found to be spliced in tandem with Δex15 and/or with Δex18. Similarly, we found Δ4–6 spliced in tandem with Δex18. Notably, both exon 15 (encodes glycosylation domain) and exon 18 (cytoplasmic insert) demonstrate a high prevalence of being excluded in the human cerebral cortex of ~25 and 50%, respectively (Gallo et al., 2022). The glycosylation domain has been shown to regulate Apoer2 extracellular processing as this region contains the cleavage site for matrix metalloproteases. Exclusion of both glycosylation domain and cytoplasmic insert in the mouse brain has been shown to affect Apoer2 cell surface levels, synaptic strength, and long-term potentiation (Wasser et al., 2014).

This study is a focused experimental approach to identify N-terminal APOER2 variants and to test for differences in APOER2 cleavage as a biological avenue to assess for function. Future experiments are under way to determine the biological function of entire APOER2 transcripts, specifically determining the localization of *APOER2* isoforms in cell types across the brain. In particular, because APOER2 plays different roles in development through interactions with ligands such as Reelin, it will be interesting to compare the distribution of APOER2 splicing in the developing brain. The APOER2 splicing landscape may be entirely different compared with the adult brain, specifically as it relates to aging and disease.

References

Azevedo OGR, Oliveira RAC, Oliveira BC, Zaja-Milatovic S, Araújo CV, Wong DVT, Costa TB, Lucena HBM, Lima RCP Jr, Ribeiro RA, Warren CA, Lima AÂM, Vitek MP, Guerrant RL, Oriá RB (2012) Apolipoprotein E COG 133 mimetic peptide improves 5-fluorouracil-induced intestinal mucositis. BMC Gastroenterol 12:35.

Bal M, Leitz J, Reese AL, Ramirez DMO, Durakoglugil M, Herz J, Monteggia LM, Kavalali ET (2013) Reelin mobilizes a VAMP7-dependent synaptic vesicle pool and selectively augments spontaneous neurotransmission. Neuron 80:934–946.

Beffert U, Weeber EJ, Durudas A, Qiu S, Masiulis I, Sweatt JD, Li W-P, Adelmann G, Frotscher M, Hammer RE, Herz J (2005) Modulation of synaptic plasticity and memory by Reelin involves differential splicing of the lipoprotein receptor Apoer2. Neuron 47:567–579.

Beffert U, Nematollah Farsian F, Masiulis I, Hammer RE, Yoon SO, Giehl KM, Herz J (2006) ApoE receptor 2 controls neuronal survival in the adult brain. Curr Biol 16:2446–2452.

Biederer T, Cao X, Südhof TC, Liu X (2002) Regulation of APP-dependent transcription complexes by Mint/X11s: differential functions of Mint isoforms. J Neurosci 22:7340–7351.

Brandes C, Novak S, Stockinger W, Herz J, Schneider WJ, Nimpf J (1997) Avian and murine LR8B and human apolipoprotein E receptor 2: differentially spliced products from corresponding genes. Genomics 42:185–191.

Brandes C, Kahr L, Stockinger W, Hiesberger T, Schneider WJ, Nimpf J (2001) Alternative splicing in the ligand binding domain of mouse ApoE receptor-2 produces receptor variants binding reelin but not alpha 2-macroglobulin. J Biol Chem 276:22160–22169.

Cao X, Südhof TCS (2001) A transcriptively active complex of APP with Fe65 and histone acetyltransferase Tip60. Science 293:115–120.

Chaufty J, Sullivan SE, Ho A (2012) Intracellular amyloid precursor protein sorting and amyloid- secretion are regulated by src-mediated phosphorylation of Mint2. J Neurosci 32:9613–9625.

Chen Y, Beffert U, Ertunc M, Tang T-S, Kavalali ET, Bezprozvanny I, Herz J (2005) Reelin modulates NMDA receptor activity in cortical neurons. J Neurosci 25:8209–8216.

Clatworthy AE, Stockinger W, Christie RH, Schneider WJ, Nimpf J, Hyman BT, Rebeck GW (1999) Expression and alternate splicing of apolipoprotein E receptor 2 in brain. Neuroscience 90:903–911.

D'Arcangelo G, Homayouni R, Keshvara L, Rice DS, Sheldon M, Curran T (1999) Reelin is a ligand for lipoprotein receptors. Neuron 24:471–479.

Dlugosz P, Nimpf J (2018) The reelin receptors apolipoprotein E receptor 2 (ApoER2) and VLDL receptor. Int J Mol Sci 19:3090.

Fisher C, Abdul-Aziz D, Blacklow SC (2004) A two-module region of the low-density lipoprotein receptor sufficient for formation of complexes with apolipoprotein E ligands. Biochemistry 43:1037–1044.

Gallo CM, Ho A, Beffert U (2020) ApoER2: functional tuning through splicing. Front Mol Neurosci 13:144.

Gallo CM, Labadorf AT, Ho A, Beffert U (2022) Single molecule, long-read Apoer2 sequencing identifies conserved and species-specific splicing patterns. Genomics 114:110318.

Gotthardt M, Trommsdorff M, Nevitt MF, Shelton J, Richardson JA, Stockinger W, Nimpf J, Herz J (2000) Interactions of the low-density lipoprotein receptor gene family with cytosolic adaptor and scaffold proteins suggest diverse biological functions in cellular communication and signal transduction. J Biol Chem 275:25616–25624.

Grehan S, Tse E, Taylor JM (2001) Two distal downstream enhancers direct expression of the human apolipoprotein E gene to astrocytes in the brain. J Neurosci 21:812–822.

GTEx Consortium (2015) The Genotype-Tissue Expression (GTEx) pilot analysis: multitissue gene regulation in humans. Science 348:648–660.

He X, Cooley K, Chung CHY, Dashti N, Tang J (2007) Apolipoprotein receptor 2 and X11 apha/beta mediate apolipoprotein E-induced endocytosis of amyloid-beta precursor protein and beta-secretase, leading to amyloid-beta production. J Neurosci 27:4052–4060.

Hibi T, Mizutani M, Baba A, Hattori M (2009) Splicing variations in the ligand-binding domain of ApoER2 results in functional differences in the binding properties to Reelin. Neurosci Res 63:251–258.

Ho A, Morishita W, Atasoy D, Liu X, Tabuchi K, Hammer RE, Malenka RC, Südhof TC (2006) Genetic analysis of Mint/X11 proteins: essential presynaptic functions of a neuronal adaptor protein family. J Neurosci 26:13089–13101.

Hoe H-S, Rebeck GW (2005) Regulation of ApoE receptor proteolysis by ligand binding. Brain Res Mol Brain Res 137:31–39.

Hoe H-S, Magill LA, Guenette S, Fu Z, Vicini S, Rebeck GW (2006) FE65 interaction with the ApoE receptor ApoER2. J Biol Chem 281:24521–24530.

Huang Y-WA, Zhou B, Wernig M, Südhof TC (2017) ApoE2, ApoE3, and ApoE4 differentially stimulate APP transcription and Aβ Secretion. Cell 168:427–441.e21.

Kavalali ET, Klingauf J, Tsien RW (1999) Activity-dependent regulation of synaptic clustering in a hippocampal culture system. Proc Natl Acad Sci U S A 96:12893–12900.

Kim DH, Iijima H, Goto K, Sakai J, Ishii H, Kim HJ, Suzuki H, Kondo H, Saeki S, Yamamoto T (1996) Human apolipoprotein E receptor 2. A novel lipoprotein receptor of the low density lipoprotein receptor family predominantly expressed in brain. J Biol Chem 271:8373–8380.

Koch S, Strasser V, Hauser C, Fasching D, Brandes C, Bajari TM, Schneider WJ, Nimpf J (2002) A secreted soluble form of ApoE receptor 2 acts as a dominant-negative receptor and inhibits Reelin signaling. EMBO J 21:5996–6004.

Laskowitz DT, Thekdi AD, Thekdi SD, Han SKD, Myers JK, Pizzo SV, Bennett ER (2001) Downregulation of microglial activation by Apolipoprotein E and ApoE-mimetic peptides. Exp Neurol 167:74–85.

Latypova EM, Timoshenko SI, Kislik GA, Vitek MP, Schwarzman AL, Sarantseva SV (2014) Investigation of neuroprotective activity of apolipoprotein E peptide mimetic Cog1410 in transgenic lines of *Drosophila melanogaster*. Biomed Khim 60:515–521.

Lynch JR, Tang W, Wang H, Vitek MP, Bennett ER, Sullivan PM, Warner DS, Laskowitz DT (2003) APOE genotype and an ApoE-mimetic peptide modify the systemic and central nervous system inflammatory response. J Biol Chem 278:48529–48533.

Mahley R (1988) Apolipoprotein E: cholesterol transport protein with expanding role in cell biology. Science 240:622–630.

Martínez-Oliván J, Arias-Moreno X, Velazquez-Campoy A, Millet O, Sancho J (2014) LDL receptor/lipoprotein recognition: endosomal weakening of ApoB and ApoE binding to the convex face of the LR5 repeat. FEBS J 281:1534–1546.

May P, Bock HH, Nimpf J, Herz J (2003) Differential glycosylation regulates processing of lipoprotein receptors by γ-secretase. J Biol Chem 278:37386–37392.

Minami SS, Sung YM, Dumanis SB, Chi SH, Burns MP, Ann E-J, Suzuki T, Turner RS, Park H-S, Pak DTS, Rebeck GW, Hoe H-S (2010) The cytoplasmic adaptor protein X11α and extracellular matrix protein Reelin regulate ApoE receptor 2 trafficking and cell movement. FASEB J 24:58–69.

Myant NB (2010) Reelin and apolipoprotein E receptor 2 in the embryonic and mature brain: effects of an evolutionary change in the apoER2 gene. Proc Biol Sci 277:345–351.

Novak S, Hiesberger T, Schneider WJ, Nimpf J (1996) A new low-density lipoprotein receptor homologue with 8 ligand binding repeats in brain of chicken and mouse. J Biol Chem 271:11732–11736.

Pitas RE, Boyles JK, Lee SH, Hui D, Weisgraber KH (1987) Lipoproteins and their receptors in the central nervous system. Characterization of the lipoproteins in cerebrospinal fluid and identification of apolipoprotein B,E (LDL) receptors in the brain. J Biol Chem 262:14352–14360.

Qiu S, Zhao LF, Korwek KM, Weeber EJ (2006) Differential reelin-induced enhancement of NMDA and AMPA receptor activity in the adult hippocampus. J Neurosci 26:12943–12955.

Rudenko G, Henry L, Henderson K, Ichtchenko K, Brown MS, Goldstein JL, Deisenhofer J (2002) Structure of the LDL receptor extracellular domain at endosomal pH. Science 298:2353–2358.

Sadowski I, Ma J, Triezenberg S, Ptashne M (1988) GAL4-VP16 is an unusually potent transcriptional activator. Nature 335:563–564.

Stockinger W, Brandes C, Fasching D, Hermann M, Gotthardt M, Herz J, Schneider WJ, Nimpf J (2000) The reelin receptor ApoER2 recruits JNK-interacting proteins-1 and -2. J Biol Chem 275:25625–25632.

Telese F, Ma Q, Perez PM, Notani D, Oh S, Li W, Comoletti D, Ohgi KA, Taylor H, Rosenfeld MG (2015) LRP8-reelin-regulated neuronal enhancer signature underlying learning and memory formation. Neuron 86:696–710.

Trommsdorff M, Gotthardt M, Hiesberger T, Shelton J, Stockinger W, Nimpf J, Hammer RE, Richardson JA, Herz J (1999) Reeler/disabled-like disruption of neuronal migration in knockout mice lacking the VLDL receptor and ApoE receptor 2. Cell 97:689–701.

Vitek MP, Christensen DJ, Wilcock D, Davis J, Van Nostrand WE, Li FQ, Colton CA (2012) APOE-mimetic peptides reduce behavioral deficits, plaques and tangles in Alzheimer's disease transgenics. Neurodegener Dis 10:122–126.

von Arnim CAF, Kinoshita A, Peltan ID, Tangredi MM, Herl L, Lee BM, Spoelgen R, Hshieh TT, Ranganathan S, Battey FD, Liu C-X, Bacskai BJ, Sever S, Irizarry MC, Strickland DK, Hyman BT (2005) The low-density lipoprotein receptor-related protein (LRP) is a novel β-secretase (BACE1) substrate. J Biol Chem 280:17777–17785.

Wasser CR, Masiulis I, Durakoglugil MS, Lane-Donovan C, Xian X, Beffert U, Agarwala A, Hammer RE, Herz J (2014) Differential splicing and glycosylation of Apoer2 alters synaptic plasticity and fear learning. Sci Signal 7:ra113.

Weeber EJ, Beffert U, Jones C, Christian JM, Förster E, Sweatt JD, Herz J (2002) Reelin and ApoE receptors cooperate to enhance hippocampal synaptic plasticity and learning. J Biol Chem 277:39944–39952.

White CR, Garber DW, Anantharamaiah GM (2014) Anti-inflammatory and cholesterol-reducing properties of apolipoprotein mimetics: a review. J Lipid Res 55:2007–2021.

Yasui N, Nogi T, Takagi J (2010) Structural basis for specific recognition of Reelin by its receptors. Structure 18:320–331.

Yeo G, Holste D, Kreiman G, Burge CB (2004) Variation in alternative splicing across human tissues. Genome Biol 5:R74.

Zhang Y, Chen K, Sloan SA, Bennett ML, Scholze AR, O'Keeffe S, Phatnani HP, Guarnieri P, Caneda C, Ruderisch N, Deng S, Liddelow SA, Zhang C, Daneman R, Maniatis T, Barres BA, Wu JQ (2014) An RNA-sequencing transcriptome and splicing database of glia, neurons, and vascular cells of the cerebral cortex. J Neurosci 34:11929–11947.